THE UNIVERSITY OF MANITOBA

ISOPARAMETRIC, FINITE-ELEMENT BOUNDARY INTEGRAL SOLUTION OF THREE-DIMENSIONAL FIELDS

BY

GARBO JENG

A THESIS

SUBMITTED TO THE FACULTY OF GRADUATE STUDIES

IN PARTIAL FULFILLMENT OF THE REQUIREMENTS FOR THE DEGREE OF

DOCTOR OF PHILOSOPHY

DEPARTMENT OF ELECTRICAL ENGINEERING

WINNIPEG, MANITOBA

JUNE 1977

ISOPARAMETRIC, FINITE-ELEMENT BOUNDARY INTEGRAL SOLUTION OF THREE-DIMENSIONAL FIELDS

BY

GARBO JENG

A dissertation submitted to the Faculty of Graduate Studies of the University of Manitoba in partial fulfillment of the requirements of the degree of

DOCTOR OF PHILOSOPHY

To my parents

ABSTRACT

A general numerical method — an isoparametric finite-element technique — is developed for the solution of integral equation formulations of three-dimensional boundary-value field problems. In contrast to filling the region with three-dimensional elements as needed in the partial differential equation approach, in the integral formulation, elements placed on boundary surfaces only are considered. The method provides high order approximation of the unknown function over a bounding surface described by essentially two-dimensional nonplanar elements. In common with alternative procedures, the finite-element method involves the formation and the solution of a system of algebraic equations. The matrix equations are derived from the Rayleigh-Ritz procedure. The use of an isoparametric mapping permits numerical integrations over surface elements, of arbitrary shapes, to be performed over a simple two-dimensional simplex. This also makes possible the development of a fully automated general algorithm applicable to arbitrary configurations. The computer implementation is discussed. Sample test results for both scalar and vector fields are included. The variational approach is compared with the conventional constant approximation point-matching method. Comparison is also made between the point-matching and the variational methods involving identical higher-order approximating function. Results obtained indicate that the variational approach is better than the point-matching method in both cases. A successive element iterative scheme is also described to handle problems

of sizes demanding a core memory in excess of the available capacity. In summary, this work has achieved the generalization of the finite-element concept to include its application to the solution of integral equations.

LIST OF FIGURES

ACKNOWLEDGEMENTS

The author wishes to express her sincere gratitude and appreciation to her supervisor, Dr. A. Wexler, for his invaluable guidance, encouragement and assistance throughout the course of this study.

The author wishes to acknowledge gratefully Dr. F.M. Arscott, Dr. H. Lakser and Dr. N. Popplewell for their advice and suggestions. The author is also indebted to Dr. B.H. McDonald, Dr. W.N.R. Stevens and Dr. G.I. Costache for many helpful discussions.

A special thanks and appreciation are due the author's parents and fiance, Chanh-Sieu Phan, for their assistance, encouragement and understanding.

Many thanks go to the author's sister, Gar-Yei, for typing the manuscript with great care, skill and patience.

Financial support from the National Research Council of Canada is gratefully acknowledged.

CONTENTS

CHAPTER I

INTRODUCTION

In solving boundary-value field problems, two distinct approaches of solution exist: the partial differential and the boundary integral approaches. In the differential method, the behaviour of the field inside and on the boundary of the domain is described by partial differential equations. If the field distribution is the quantity of interest, the solution is obtained directly by solving the differential equations. However, if the source is to be found, it is obtained indirectly by differentiation of the field. Alternatively, one may assume a given field distribution to be represented by some form of source distributions on the boundary of the region, which are obtained as solutions of integral equations [1,2,3]. The approach is known as the boundary integral equation method. It refers to the class of methods where the governing equation is an integral equation relating the unknown function defined on the boundary only to known field quantities on the boundary.

To solve, for example, the problem of finding the potential distribution governed by the Laplace equation

$$-\nabla^2\phi = 0 \tag{1.1}$$

subject to prescribed boundary conditions, one may derive the solution from an integral formulation. Denoting by $G(p|q)$ the free-space Green's function for (1.1), in three-dimensional space, we have

$$G(p|q) = \frac{1}{4\pi|p-q|} \tag{1.2}$$

The potential at a point p may be represented by means of a single-layer source distribution σ on the boundary S in the form [4]

$$\phi(p) = \int_S G(p|q)\ \sigma(q)\ dq \tag{1.3}$$

Suppose that a Dirichlet condition

$$\phi(q) = g(q) \qquad q \in S \tag{1.4}$$

is specified on the boundary. If the source distribution σ on S is determined such that (1.4) is satisfied, the problem is solved. Applying the boundary condition (1.4), an integral formulation of the problem is given by the expression

$$\int_S G(p|q)\ \sigma(q)\ dq = g(p) \qquad p \in S \tag{1.5}$$

which is a Fredholm integral equation of the first kind.

Refering to Fig. 1.1 which depicts an interface problem. On part of the boundary the interface condition

$$\varepsilon_1 \frac{\partial\phi}{\partial n} = \varepsilon_2 \frac{\partial\phi}{\partial n} \tag{1.6}$$

is to be specified. Taking into consideration the discontinuity properties of the normal derivatives, the single-layer representation (1.3) yields a Fredholm integral equation of the second kind [25]

$$\frac{\varepsilon_1+\varepsilon_2}{2}\,\sigma(p) + (\varepsilon_1-\varepsilon_2)\int_S \sigma(q)\,\frac{\partial G}{\partial n}\,(p|q)\,dq = 0 \qquad p \in S_2 \qquad (1.7)$$

for the interface condition. Equation (1.7) together with (1.5) provides a complete integral formulation to the problem of Fig. 1.1.

In both the partial differential and the integral equation approaches, exact solution of, for example, equations (1.1), (1.5) or (1.7) by analytical techniques is usually not possible. Approximate solution by numerical methods is the natural choice. The numerical procedure involves the replacement of the continuum equation by a set of algebraic equations. The size of the matrix system is, in general, directly related to the size of the region in which the continuum operator is defined. For problems with large regions, the partial differential equation approach suffers because the unknown function is defined over the entire region. On the other hand, the integral equation method, because the problem is formulated in terms of a function on the boundary, has the advantage of requiring a smaller number of unknowns. This is particularly advantageous

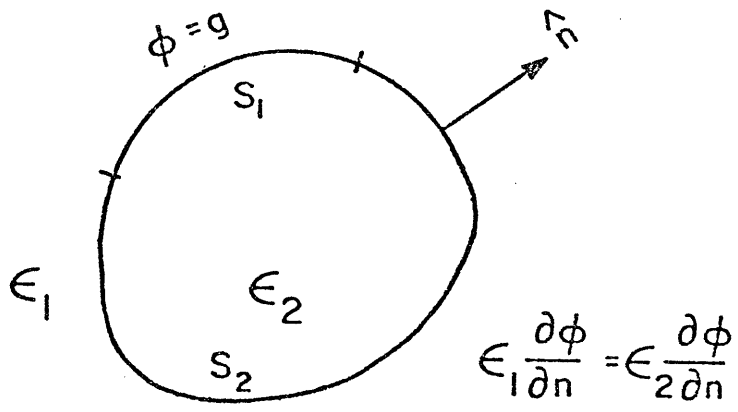

Fig. 1.1 An interface problem

in open-region problems. However, for regions containing nonuniform inhomogeneities, the integral equation formulation requires a special Green's function which is as difficult to find as solving the original problem. The method is therefore of advantage for homogeneous or uniformly inhomogeneous regions where free-space Green's functions are applicable. On the other hand, the partial differential approach handles inhomogeneities easily. Several methods have been reported for solving open-region problems. The boundary relaxation method [5,6] assumes a boundary condition on an artificial boundary, solves the partial differential formulation and updates the assumed condition iteratively through an integral relation defined on the boundary. The picture frame methods [7,8,9] use an integral equation formulation to define the field in the uniform region exterior to an artificially imposed boundary. The interior partial differential formulation and the exterior integral equation are coupled to yield a solution to the complete problem. No approximation as to boundary conditions is involved and the solution is obtained by considering the field in all space. In [7] and [8], a complete equivalent source representation comprising both the single and double layer sources is used whereas the dipole layer contribution is neglected in [9]. Moreover, in [8], two artificial boundaries are defined thus sidestepping the Green's function singularity. In general, for large problems with local inhomogeneities, it is most appropriate to use both the differential and the integral equation methods simultaneously [10].

The technology for partial differential equations is well-developed. In addition to the somewhat classical finite-difference discretization of differential operators, the finite-element discretization [11,12] based

on the variational method [13] has been proved a useful method of obtaining an approximate solution to partial differential equations. The essential idea of the method is to divide the region in which the problem is to be solved into arbitrary size of triangular or rectangular subregions (called elements), permitting a close approximation to boundary shapes. Complicated geometry can be dealt with easily. The unknown function is uniquely specified by a discrete number of its values associated with specified nodal points of the region. Then the stationarity (or minimization in the case of positive-definite operators) of the functional with respect to the nodal values yields a discretized system of equations, the solution of which gives an approximate solution to the problem.

It is evident that a higher-order approximation would yield a better representation to a continuous function than would the constant approximation. While high-order implementation plays a practical role in providing an approximate solution to problems described by partial differential equations, flat surface elements with constant values of approximation are most customarily used in solving integral equations. The method of moments [14] is the most commonly used method. Except for problems involving simple geometry and for situations where physical knowledge may furnish a special set of expansion functions, general practice is to employ pulse expansion and point-matching discretization. The procedure has been reported in the numerical solution of integral equations arising in many different fields, for example, in elasticity [15-17], sound radiation [18,19], electromagnetic radiation and scattering [20-22]. The pulse approximation to a continuous function would generally require more variables than a higher-order approximation. The former thus demands a greater computing cost

than would the latter for a solution of comparable accuracy.

Cruse [23], in his work on three-dimensional elastic stress analysis, improves upon the efficiency of pulse expansion approximation by allowing a linear variation of the function over a surface modelled in a piecewise flat sense. The discretized system of equations was derived by the point-matching approach. Silvester and Hsieh [24] described a Galerkin procedure for the solution of integral equations arising in electric and magnetic static fields. McDonald, Friedman and Wexler [25] reported a variational approach whereby convergence was guaranteed for operators having a positive-definite component [13]. It has been shown that for a self-adjoint operator, the resulting discretized system of equations are identical to those obtained from the Galerkin method. For interface problems between dissimilar media, it has also been shown [26] that the Galerkin and variational approaches correspond. For two-dimensional problems, [25] obtained the solution by a pure variational approach with a single polynomial approximation over the entire region. The approach lends equal weight to all portions of the region. For three-dimensional problems, only pulse expansion approximation over piecewise flat surfaces was previously available.

In this work, the finite-element method is established for the solution of boundary integral equations for three-dimensional fields. The technique is a natural extension of the isoparametric finite-element method commonly used for the solution of partial differential equations. It permits piecewise polynomial approximations to the unknown function and allows high-order modelling of curved surfaces with a consequent reduction in the significant but often neglected geometrical modelling error. The use of an isoparametric mapping, which enables all numerical integrations

to be performed over a two-dimensional simplex, facilitates the development of a package of FORTRAN computer programs applicable to problems of arbitrary configuration. The above-mentioned method is described in Chapter II.

Lachat and Watson [27] described a related method for elastic analysis using a parametric representation for both the function and the geometry. The matrix equation was derived from a point-matching discretization. Moreover, a banded system was assumed. In the finite-element solution of a partial differential equation, a sparse matrix results from subdivision of the region, whereas for integral equations, because integral operators account for mutual interaction between all pairs of elements, the resulting matrix is dense. For computational economy, simplifying approximations, such as neglecting the effect of distant elements and hence setting the corresponding matrix entries to zero, may be made. However, such approximations are *ad hoc* and must be justified on an individual basis. Unfortunately, reference [27] gave no discussion to the occurence of the banded system. A successive element iterative scheme is described in Chapter II for the solution of large problems.

In Chapter III, Dirichlet problems of electrostatics are formulated as Fredholm integral equations of the first kind and are solved by the finite-element method. In Chapter IV, the integral finite-element method is demonstrated by solving a Fredholm integral equation of the second kind with a magnetic scalar potential. It is shown that the single-field formulation yields an ill-conditioned formulation in computing field values in the region exterior to the permeable body. An integration

scheme, analogous to that used in the isoparametric finite-element approach of Chapter II, is described for the volume integration involved in the computation of magnetic field due to current sources.

Chapter V describes the method for vector fields. In particular, the displacement problem of elasticity is considered. In summary, the object of this presentation is to introduce a novel numerical method — the boundary integral finite-element method — for the solution of boundary integral equations. Its applicability is demonstrated with both scalar and vector solutions of Fredholm integral equations of the first and the second kinds covering the most frequently encountered formulations in engineering applications.

CHAPTER II

FINITE ELEMENT SOLUTION OF INTEGRAL EQUATIONS

The essence of numerical solution of integral equations is to transform the integral operator equations to a system of algebraic equations which can then be solved by standard procedures [30]. The most commonly used method for such a transformation is the method of moments with pulses for the expansion functions and delta functions for the testing functions [14]. The method replaces the curved or flat boundary by N planar subregions over each of which the unknown function is assumed to be constant. One then constrains the integral equation to hold at N points on the boundary, thus obtaining a set of N linear algebraic equations to solve for the N constant function values. Such approximations, although fairly easy to implement, are unnecessarily crude.

In this chapter, an isoparametric finite-element method is presented for solving boundary integral equations of three-dimensional fields. First, a systematic approach to derive a variational formulation for nonself-adjoint operator equations is described. The method, based on the well-developed finite-element method for two-dimensional partial differential equations with extension to deal with an arbitrary surface in space, is derived. Special singularity treatment required for the kernel of the integral operators is described. Furthermore, an iterative scheme is presented which provides an alternative approach to cater for large problems. Finally, the computer implementation is discussed.

2.1 THE FUNCTIONAL

Consider the operator equation

$$K\sigma = g \tag{2.1}$$

where K is a real integral operator defined by $K\ldots = \int K(s|s')\ldots ds'$. Assume that there is an adjoint operator, K^a, to the operator K with the property

$$< K\sigma,\tau > = < \sigma,K^a\tau > \tag{2.2}$$

where the pair of brackets is defined by [31]

$$< u,v > = \int uv^* \, ds \tag{2.3}$$

The superscript * denotes the complex-conjugate. An operator, K, is said to be self-adjoint if

$$< K\sigma,\tau > = < \sigma,K\tau > \tag{2.4}$$

Equation (2.4) follows directly from (2.2) if K is self-adjoint, that is, if $K = K^a$. It can easily be verified that the integral operator of (2.1) is self-adjoint if the kernel, $K(s|s')$, satisfies the relation

$$K(s|s') = K(s'|s) \tag{2.5}$$

That is, self-adjointness of an integral operator requires the kernel be symmetric. In general, the adjoint operator of a complex integral operator is one with the kernel being replaced by its complex-conjugate transpose.

The well-known stationary principle [13] states that for a self-adjoint operator K, if σ_o is such that $K\sigma_o=g$, then the functional

$$F = < K\sigma,\sigma > - < \sigma,g > - < g,\sigma > \quad \text{(for complex } \sigma \text{ and/or g)} \tag{2.6}$$

or

$$F = < K\sigma,\sigma > - 2< \sigma,g > \quad \text{(for the real case)} \tag{2.7}$$

is stationary at $\sigma=\sigma_o$.

If K is nonself-adjoint and if σ_o and τ_o are such that $K\sigma_o=g$ and $K^a\tau_o=h$, then the functional

$$F = < K\sigma,\tau > - < g,\tau > - < \sigma,h > \tag{2.8}$$

is stationary at $\sigma=\sigma_o$ and $\tau=\tau_o$.

The proof is direct. Let $\sigma=\sigma_o+\xi$ and $\tau=\tau_o+\eta$, then

$$\begin{aligned} F(\sigma,\tau) &= F(\sigma_o+\xi,\tau_o+\eta) \\ &= < K\sigma_o,\tau_o > + < K\xi,\tau_o > + < K\sigma_o,\eta > + < K\xi,\eta > \\ &\quad - < g,\tau_o > - < g,\eta > - < \sigma_o,h > - < \xi,h > \end{aligned} \tag{2.9}$$

Also,

$$F(\sigma_o,\tau_o) = < K\sigma_o,\tau_o > - < g,\tau_o > - < \sigma_o,h > \tag{2.10}$$

Therefore

$$F(\sigma,\tau) - F(\sigma_o,\tau_o) = < K\xi,\eta > \tag{2.11}$$

Since $< K\xi,\eta >$ is second order in ξ,η, $F(\sigma,\tau)$ is stationary about $\sigma=\sigma_o$ and $\tau=\tau_o$.

By taking the approximating functions σ and τ to be

$$\sigma = \underline{\sigma}^T \underline{\alpha} = \underline{\alpha}^T \underline{\sigma} \tag{2.12}$$

and

$$\tau = \underline{\tau}^T \underline{\alpha} = \underline{\alpha}^T \underline{\tau} \tag{2.13}$$

where $\underline{\alpha}$ is a vector of interpolating functions and $\underline{\sigma}$ and $\underline{\tau}$ contain the variational parameters, the functional given by (2.8) produces

$$F = \underline{\sigma}^T < K\underline{\alpha}, \underline{\alpha}^T > \underline{\tau} - < g, \underline{\alpha}^T > \underline{\tau} - \underline{\sigma}^T < \underline{\alpha}, h > \tag{2.14}$$

Upon taking the variation with respect to $\underline{\tau}$, (2.14) results in a system of equations

$$< K\underline{\alpha}, \underline{\alpha}^T > \underline{\sigma} = < g, \underline{\alpha} > \tag{2.15}$$

which is algorithmically identical to that obtained from Galerkin's method. It may also be noted that by taking the set of approximating functions to be

$$\sigma = \underline{\sigma}^T \underline{\alpha} = \underline{\alpha}^T \underline{\sigma} \tag{2.16}$$

and

$$\tau = \underline{\tau}^T \underline{\beta} = \underline{\beta}^T \underline{\tau} \ , \tag{2.17}$$

the system of equations (2.15) is

$$< K\underline{\alpha}, \underline{\beta}^T > \underline{\sigma} = < g, \underline{\beta} > \tag{2.18}$$

which is the system of equations resulting from the moment method in general.

Expressing explicitly, the functional (2.8) for the integral operator

$$K\sigma(s) = p\sigma(s) + \int K(s|s')\,\sigma(s')\,ds' \tag{2.19}$$

is

$$F = \int \tau^*(s)\,[p\sigma(s) + \int K(s|s')\sigma(s')ds']\,ds - \int g(s)\tau^*(s)\,ds - \int h^*(s)\sigma(s)\,ds \tag{2.20}$$

If $K(s|s') = K(s'|s)$, (2.20) reduces to, for real σ and g,

$$F = \int \sigma(s)\,[p\sigma(s) + \int K(s|s')\sigma(s')ds']\,ds - 2\int g(s)\sigma(s)\,ds \tag{2.21}$$

In the following section, the finite-element discretization is described for obtaining the Rayleigh-Ritz equations.

2.2 FINITE ELEMENTS AND THE RAYLEIGH-RITZ PROCEDURE

The finite-element method using Rayleigh-Ritz procedure [32] provides an efficient technique for finding the stationary point of the functional (2.20). The detail of the method for partial differential operators is given in [11,12].

The basic philosophy of the method is the division of the region of interest into smaller regions (elements) over each of which the unknown function is represented by an appropriate trial function. A further important feature is that it permits one element to be considered at a time resulting in algorithmic generality and simplicity. The variational method in its pure form, on the other hand, represents the unknown function by a

trial function defined over the entire region of interest.

Now, suppose the region where the unknown function is defined is divided into triangular subregions as shown in Fig. 2.1. Over each element, the unknown, say f, is assumed to vary in a polynomial fashion, in contrast to the pulse approximation used in [25], for example. Furthermore, this variation is expressed in terms of the M element nodal values as

$$f_k = \sum_{i=1}^{M} \alpha_i f_{ki} \tag{2.22}$$

where the subscript k refers to the kth element, f_{ki} being the ith nodal value of the kth element and

$$M = \frac{1}{2}(N+1)(N+2) \tag{2.23}$$

for a degree N approximation.

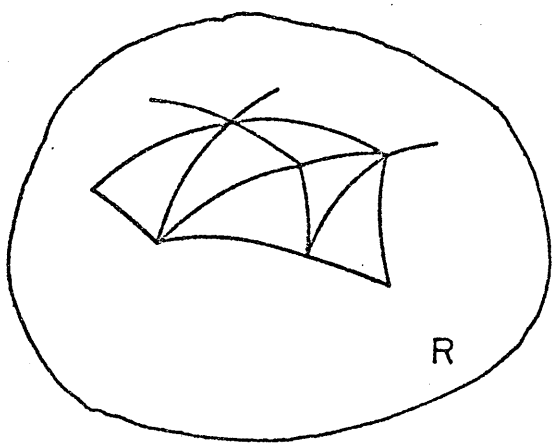

Fig. 2.1 Finite-element subdivision of a region

The α_i terms are the appropriate interpolatory functions, known as the shape functions, which by definition takes on the values

$$\alpha_i = \begin{cases} 1 & \text{at node } i \\ 0 & \text{at other nodes.} \end{cases} \tag{2.24}$$

For a first order approximation (N=1) in two variables, we have M = 3. The three unknown parameters are the nodal values at the three vertices of the triangular element. Hence along each side of the element, the first order approximation is uniquely determined by the two nodal values. This ensures continuity of the function across the common side of two adjacent elements. Similarly, for N = 2, the six nodal variables are placed as shown in Fig. 2.2, having three values along each side to uniquely specify a second order approximation.

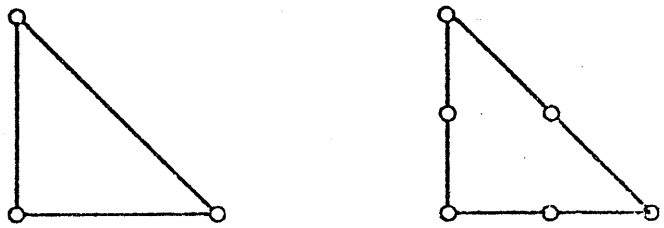

N=1 N=2

Fig. 2.2
Node arrangements in elements

In vector notation, (2.22) is

$$f_k = \underline{\alpha}^T \underline{f}_k = \underline{f}_k^T \underline{\alpha} \tag{2.25}$$

where the superscript T denotes the transpose, $\underline{\alpha}^T = [\alpha_1, \alpha_2, \ldots, \alpha_M]$ and $\underline{f}_k^T = [f_{k1}, f_{k2}, \ldots, f_{kM}]$.

The functional contribution from element k is obtained by substituting (2.25) into (2.21), for example, we get

$$F_k = \underline{f}_k^T \int_{S_k} p\underline{\alpha}(s)\underline{\alpha}^T(s)\, ds\, \underline{f}_k + \sum_{t=1}^{n} \underline{f}_k^T \left[\int_{S_k} \underline{\alpha}(s) \int_{S_t} K(s|s')\underline{\alpha}^T(s')\, ds'ds\right] \underline{f}_t - 2\underline{f}_k^T \int_{S_k} g(s)\underline{\alpha}(s)\, ds \qquad (2.26)$$

where n is the total number of elements. For a subdivided region, (2.26) is applied to each element in turn and sum to yield the total contribution

$$F = \sum_{i=1}^{n} F_i \qquad (2.27)$$

The stationary point of F and, thus, the solution of the operator equation is obtained by differentiating F with respect to each variational parameter and setting each resulting equation to zero, i.e.,

$$\frac{\partial F}{\partial \underline{f}_i} = 0\ , \qquad i = 1,2,\ldots,n. \qquad (2.28)$$

From (2.26) and (2.27), (2.28) is a system of equations of the form

$$S\underline{f} = \underline{b} \qquad (2.29)$$

where S is an NxN dense matrix (N being the total number of nodes), $\underline{f}$ an Nx1 vector of the unknowns and $\underline{b}$ an Nx1 known vector. The elements of S

and $\underline{b}$ are given, respectively, by

$$S_{ij} = \sum_{\ell \varepsilon V_{ij}} \int \alpha_{p_{\ell i}}(s)\, \alpha_{p_{\ell j}}(s)\, ds + \sum_{\ell \varepsilon V_i} \int_{S_\ell} \alpha_{p_{\ell i}}(s) \sum_{k \varepsilon V_j} \int_{S_k} K(s|s')\, \alpha_{p_{kj}}(s')\, ds' ds \qquad (2.30)$$

$$b_i = \sum_{\ell \varepsilon V_i} \int_{S_\ell} g(s)\, \alpha_{p_{\ell i}}(s)\, ds \qquad (2.31)$$

where $p_{\ell i}$ is the local node number within element ℓ of node i. V_i is the set of elements sharing node i as one of the nodes and V_{ij} is the set of elements having both i and j as its nodes.

One should note here one of the essential differences between the finite-element discretization of partial differential formulations and integral formulations. Since the integral operation accounts for the mutual interaction between pairs of elements, the off-diagonal entries of the coefficient matrix S in (2.29) are completely filled. Whereas in the partial differential discretization, only nodes connected to elements that are adjacent to the element under consideration contributes to non-vanishing off-diagonal entries in the corresponding S matrix. A sparse matrix therefore results from the subdivision of the region and moreover, a banded system may be obtained by an appropriate numbering of the nodes.

For computational economy, simplifying assumptions, such as neglecting the effect of distant elements and hence setting the corresponding matrix entries to zero, may be made in the integral case. However, it is to be emphasized that such approximations are *ad hoc* and must be justified

on an individual basis. A banded system was assumed in the work on elastic analysis by Lachat and Watson [27]. Unfortunately, no explanation was given for the occurance of the banded matrix.

2.3 ISOPARAMETRIC INTEGRAL ELEMENTS

Consider an arbitrary surface S in space over which the integral operator is defined. The finite-element method described in Section 2.2 enables one to divide S into subregions and to treat each subregion individually.

Now, in contrast to the common procedure of approximating the region by piecewise flat surfaces in the numerical solution of integral equations, a parametric representation is used which yields high-order approximations.

Referring to Fig. 2.3, a local coordinate system ξ-η and the global coordinate system x-y-z are defined as shown. A mapping from the local coordinates to the global coordinates is derived by assuming each global coordinate to be a polynomial function of the local coordinates. Expressing this polynomic variation in terms of the M node-points on the surface and restricting the elements in the global system to correspond to the two-dimensional simplex defined by the vertices (0,1), (0,0) and (1,0), we have

$$x = \sum_{i=1}^{M} \alpha_i(\xi,\eta)\, x_i$$

$$y = \sum_{i=1}^{M} \alpha_i(\xi,\eta)\, y_i \qquad (2.32)$$

and $$z = \sum_{i=1}^{M} \alpha_i(\xi,\eta)\, z_i$$

where M and α are defined as in (2.23) and (2.24), and (x_i, y_i, z_i) are the global coordinates of node i. Expressions (2.32) are essentially parametric equations defining a family of surfaces in space. By taking the α functions to be linear in ξ and η, the surface S is a plane triangle in space. For piecewise linear boundary surfaces, this finite-element model is exact and the linear mapping is sufficient. However, the mapping provided by (2.32) allows elements in the global system to be nonplanar. With higher-order terms in α, the global surface can assume any reasonable curvature in order to provide a good representation of the surface.

Table 2.1 summarizes the shape functions for the first and the second order approximations.

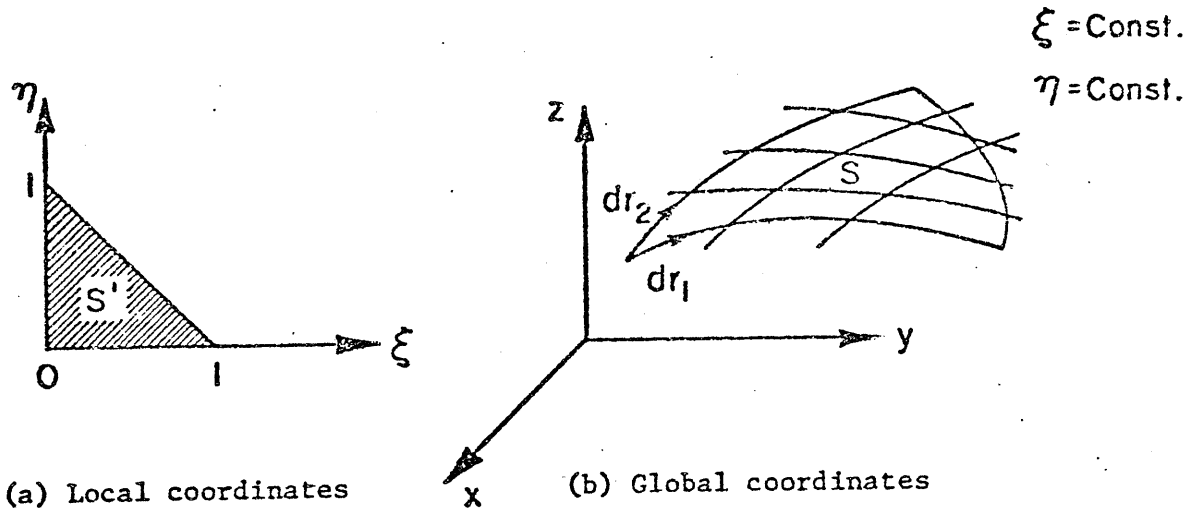

Fig. 2.3 (a) The simplex element and
(b) its transformation to the three-space

TABLE 2.1

The shape functions $\alpha_i(\xi,\eta)$

i	N=1	N=2
1	η	$\eta(2\eta-1)$
2	$1-\xi-\eta$	$(1-\xi-\eta)(1-2\xi-2\eta)$
3	ξ	$\xi(2\xi-1)$
4		$4\eta(1-\xi-\eta)$
5		$4\xi(1-\xi-\eta)$
6		$4\xi\eta$

To integrate (2.30) and (2.31) over the simplex, one must obtain the expression for the differential area. Differential changes in position in x-y-z due to changes in ξ-η are

$$\bar{dr}_1(\xi) = \frac{\partial x}{\partial \xi} d\xi\, \hat{i} + \frac{\partial y}{\partial \xi} d\xi\, \hat{j} + \frac{\partial z}{\partial \xi} d\xi\, \hat{k}$$

and (2.33)

$$\bar{dr}_2(\eta) = \frac{\partial x}{\partial \eta} d\eta\, \hat{i} + \frac{\partial y}{\partial \eta} d\eta\, \hat{j} + \frac{\partial z}{\partial \eta} d\eta\, \hat{k}$$

The differential area is

$$\bar{ds} = \bar{dr}_1 \times \bar{dr}_2 \tag{2.34}$$

From (2.33) and (2.34), the transformation factor between the two-dimensional simplex and a surface in space is

$$J = \sqrt{M_{31}^{\,2} + M_{32}^{\,2} + M_{33}^{\,2}} \tag{2.35}$$

where the M_{ij} terms are the minors of

$$A_{ij} = \begin{bmatrix} \frac{\partial x}{\partial \xi} & \frac{\partial y}{\partial \xi} & \frac{\partial z}{\partial \xi} \\ \frac{\partial x}{\partial \eta} & \frac{\partial y}{\partial \eta} & \frac{\partial z}{\partial \eta} \\ 1 & 1 & 1 \end{bmatrix} \tag{2.36}$$

taken along the bottom row. In the special case of ξ-η simplex to two-dimensional x-y plane mapping, the above transformation reduces to the familiar form used for two-dimensional isoparametric elements in solving partial differential equations. The Jacobian of transformation in this case is

$$J = \begin{vmatrix} \frac{\partial x}{\partial \xi} & \frac{\partial y}{\partial \xi} \\ \frac{\partial x}{\partial \eta} & \frac{\partial y}{\partial \eta} \end{vmatrix} \tag{2.37}$$

Now, for the unknown function f, instead of approximating it by piecewise constant or linear variation commonly used in the numerical solution of integral equations, the finite-element method developed here allows f to vary in a polynomial fashion. Furthermore, analogous to the geometric representation, the variation of f is represented in terms of the shape functions and the nodal values of the function which are yet to be determined. Therefore

$$f_k = \sum_{i=1}^{M} \alpha_i f_{ki} \tag{2.38}$$

where the subscript k denotes the kth subregion and f_{ki} terms are the

unknown nodal values. The elements so defined ensure continuity of the function along the interfaces of adjacent elements.

2.4 EVALUATION OF THE MATRIX ENTRIES

To generate the S matrix of (2.29), from (2.30) a typical integral of the form

$$\int_{S_k} \alpha_i(p) \int_{S_t} K(p|q)\ \alpha_j(q)\ ds_q ds_p \tag{2.39}$$

is to be evaluated. It involves the evaluation of a double surface integral. The isoparametric mapping of the previous section allows the integration to be performed over a simplex. To do this, the integrand of (2.39) has to be evaluated at a specific set of points over ξ-η. For any given point in the local system, the corresponding image points in the global system are easily found with (2.32) and so, in effect, $G(\xi,\eta|\xi',\eta')\ \alpha(\xi',\eta')$ is known.

The algorithm for performing the double integration will now be described. Suppose the regions of integrations for the outer and the inner integrals are S_1 and S_2, respectively, as shown in Fig. 2.4.

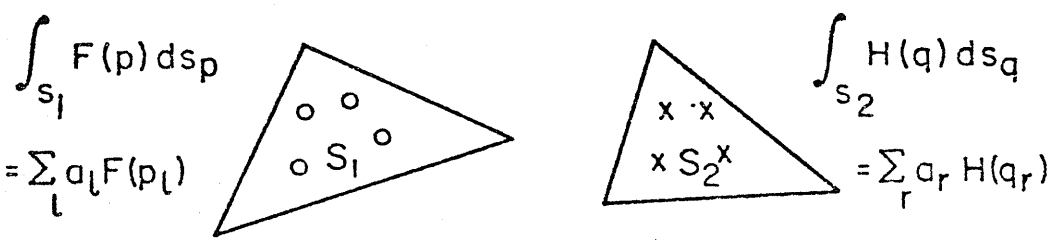

Fig. 2.4 Integration regions and sampling points

Applying the quadrature formula [33] to evaluate the integral (2.39), we have

$$\int_{S_1} \alpha_i(p) \left[\int_{S_2} K(p|q)\ \alpha_j(q)\ ds_q\right] ds_p = \sum_{\ell=1}^{n} a_\ell\ F(p_\ell) \tag{2.40}$$

where p_ℓ and a_ℓ, $\ell = 1,2,\ldots,n$ are the sampling points and the weights, respectively, of the quadrature formula used. $F(p_\ell)$ is the function value at $p = p_\ell$ of the integrand for the outer integral, i.e.,

$$F(p_\ell) = \alpha_i(p_\ell) \int_{S_2} K(p_\ell|q)\ \alpha_j(q)\ ds_q \tag{2.41}$$

If F(p) were an explicit expression in p, straightforward substitution of $p = p_\ell$ gives the value of $F(p_\ell)$ directly. An approximate value for the integral (2.40) is thus obtained as the sum of the product of the weight and the function value $F(p_\ell)$ at each sampling point p_ℓ, $\ell = 1,2,\ldots,n$.

However, $F(p_\ell)$ as given by (2.41) involves an integration over S_2, i.e., the integration

$$H(p_\ell) = \int_{S_2} K(p_\ell|q)\ \alpha(q)\ ds_q \tag{2.42}$$

which is yet to be evaluated. Once $H(p_\ell)$ is found, $F(p_\ell)$ is known from

$$F(p_\ell) = \alpha(p_\ell)\ H(p_\ell) \tag{2.43}$$

Now, consider $K(p_\ell|q)$ being a function which is singular at $q = p_\ell$ and is of the form

$$K(p_\ell|q) = \frac{1}{|q-p_\ell|} \tag{2.44}$$

One then requires the evaluation of

$$H(p_\ell) = \int_{S_2} \frac{\alpha(q)}{|q-p_\ell|}\, ds_q \tag{2.45}$$

In nearly all practical situations, it is not possible to integrate (2.45) analytically. Hence, numerical quadrature is needed. The integrand of (2.45) is a well-behaved regular function if the point p_ℓ lies outside of the region of integration S_2. In this case, a quadrature formula can be applied to yield an approximate value to $H(p_\ell)$, that is

$$H(p_\ell) = \sum_{r=1}^{n} a_r\, h(q_r) \tag{2.46}$$

where q_r is the rth sampling point for the region S_2, a_r the corresponding weight at q_r, and $h(q_r) = \alpha(q_r)/|q_r-p_\ell|$. From (2.40), (2.43) and (2.46), the integral (2.39) is therefore given by

$$\int_{S_k} \alpha_i(p) \int_{S_t} K(p|q)\, \alpha_j(q)\, ds_q ds_p = \sum_{\ell=1}^{n} \sum_{r=1}^{n} a_\ell a_r\, \alpha_i(p_\ell)\, h(q_r) \tag{2.47}$$

For the regions of integrations shown in Fig. 2.4, S_1 and S_2 are not connected to each other. The point p_ℓ appearing in (2.45) does not lie in S_2. Therefore, (2.47) is always applicable directly.

When S_1 overlaps S_2, as shown in Fig. 2.5(a), p_ℓ for S_1 always lies within the region of integration S_2 for the integral $H(p_\ell)$ given by

(a) (b)

Fig. 2.5 (a) Overlapping elements
(b) Adjacent elements

(2.45). The integrand in (2.45) is singular at p_ℓ. In this case, numerical quadrature formulas expressed by (2.47), do not yield acceptable results. As a matter of fact, using the variational procedure, p_ℓ may coincide with one of the sampling points for S_2. In this case, (2.47) fails altogether due to division by zero. However, even if p_ℓ, the singular point, does not coincide with any of the sampling point, a situation frequently encountered in the point-matching approach where the matching point may be arranged so that division by zero does not occur, numerical results obtained directly from (2.47) will not be acceptable. The addition and subtraction technique [25] to be described in the following section is needed to handle the singular integrand of S_2.

In the case where S_1 and S_2 have a common side L (Fig. 2.5(b)), for any p_ℓ lying on L, the integral (2.45) over S_2 has a singular integrand. The technique of subtraction and addition which subtracts off the singular function from the integrand would then be needed for (2.45). The

integrated function H(p) of (2.45), however, is regular. The integral over S_1 therefore involves the integration of a well-behaved function. Hence, for the outer integral, numerical quadrature expressed by (2.40) always holds.

2.5 HANDLING OF KERNEL SINGULARITY

To illustrate the approach in handling the kernel singularity, consider a kernel containing a singular function of the form given by (2.44). To remove the singularity at $q = p_\ell$, the integral (2.42)

$$H(p_\ell) = \int_{S_2} K(p_\ell|q)\ \alpha(q)\ ds_q$$

is expressed as

$$\int_{S_2} [K(p_\ell|q)\ \alpha(q) - \alpha(p_\ell)\ K_s(p_\ell|q)]\ ds_q + \alpha(p_\ell) \int_{S_2} K_s(p_\ell|q)\ ds_q \tag{2.48}$$

where K_s is the singular portion of the kernel and the closed-form expression for the last integral in (2.48) is assumed to exist. The first integral in (2.48) has a regular integrand and thus can be easily evaluated numerically whereas the second integral is computed analytically.

Referring to Fig. 2.6, an orthogonal coordinate system t-u-v is defined as shown. The t-u plane is in the plane of the element and the normal direction, $\hat{n}$, is in the +v direction.

The direction cosines of $\hat{n}$ are given by

$$n_x = [(y_c-y_b)(z_a-z_b) - (y_a-y_b)(z_c-z_b)]/2\Delta$$

$$n_y = [(x_a-x_b)(z_c-z_b) - (x_c-x_b)(z_a-z_b)]/2\Delta \qquad (2.49)$$

$$n_z = [(x_c-x_b)(y_a-y_b) - (x_a-x_b)(y_c-y_b)]/2\Delta$$

where Δ is the area of the triangle abc.

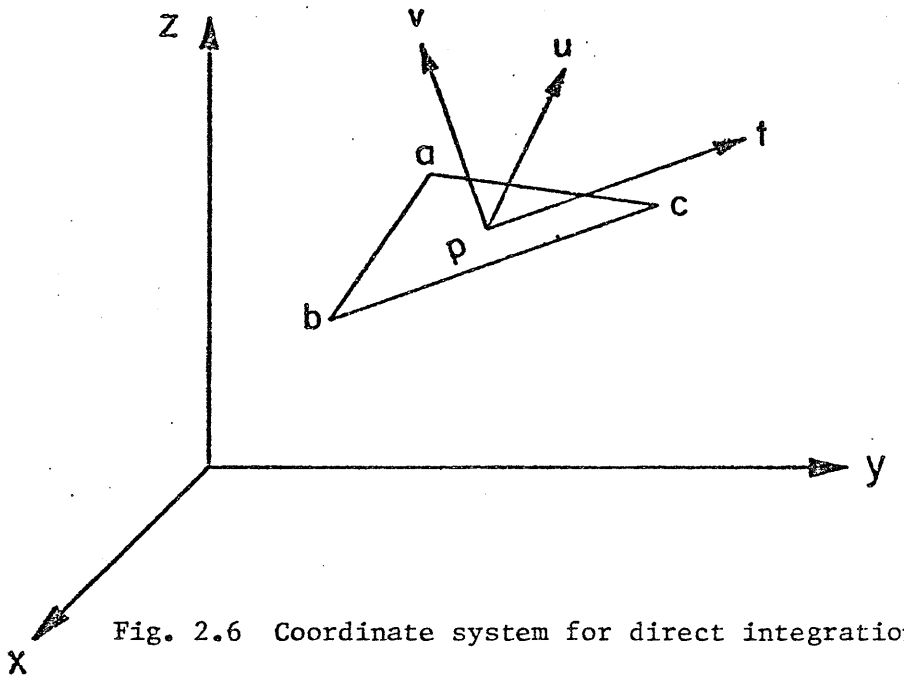

Fig. 2.6 Coordinate system for direct integration

The integral of (2.44)

$$I = \int_S \frac{1}{|\bar{r}-\bar{r}_p|}\, ds \qquad (2.50)$$

over the triangular element can therefore be written in the t-u-v coordinate system as

$$I = \int_{t_b}^{t_a} \int_{f_a(t)}^{f_c(t)} \frac{1}{\sqrt{t^2+u^2}}\, dudt + \int_{t_a}^{t_c} \int_{f_a(t)}^{f_b(t)} \frac{1}{\sqrt{t^2+u^2}}\, dudt \qquad (2.51)$$

where $f_a(t)$, $f_b(t)$ and $f_c(t)$ are the equations of the lines bc, ac and ab, respectively, in the t-u-v coordinates. Each of the integrals in (2.51) is to be evaluated analytically. Let $f(t) = mt + n$. An integral of the form

$$I' = \int_0^T \int_0^{f(t)} \frac{1}{\sqrt{t^2+u^2}}\, dudt \qquad (2.52)$$

is obtained as

$$I' = T \sinh^{-1}\left(\frac{n}{T} + m\right) + \frac{1}{\sqrt{m^2+1}} \{\ell n|\sqrt{m^2+1}\,[(m^2+1)\,T^2 + 2mnT + n^2]^{\frac{1}{2}}$$

$$+ (m^2+1)T + mn| - \ell n|\sqrt{m^2+1}\,|n| + mn|\} \qquad (2.53)$$

Equation (2.51) can therefore be computed using the expression given by (2.53).

It is relevant to remark that the applicability of (2.48) depends completely on whether the closed-form expression for the singular integral can be found. The closed-form expressions for the integral (2.50) over nonplanar domains are not readily available. In this case, the curved region of integration is approximated by a planar region and the element is defined by the three vertex nodes a, b, c (Fig. 2.6) as

$$x = \alpha_a(\xi,\eta)\ x_a + \alpha_b(\xi,\eta)\ x_b + \alpha_c(\xi,\eta)\ x_c$$

$$y = \alpha_a(\xi,\eta)\ y_a + \alpha_b(\xi,\eta)\ y_b + \alpha_c(\xi,\eta)\ y_c \qquad (2.54)$$

$$z = \alpha_a(\xi,\eta)\ z_a + \alpha_b(\xi,\eta)\ z_b + \alpha_c(\xi,\eta)\ z_c$$

where α_a, α_b and α_c being the shape functions corresponding to the first order approximation as given in Table 2.1. This introduces an error which is a function of the closeness of the planar representation to the curved region involved in the second integral of (2.48). To obtain a reasonable representation, in evaluating the second integral, quadratic regions of integration are approximated by four planar subregions defined by the six nodes of an element as shown in Fig. 2.7. This is a convenient and systematic scheme as the subdivision is obtained with existing element nodes and, hence, no extra data is required and can be easily programmed. The approximation has been found to give adequate results. However, should a better approximation be needed, a finer subdivision may be used.

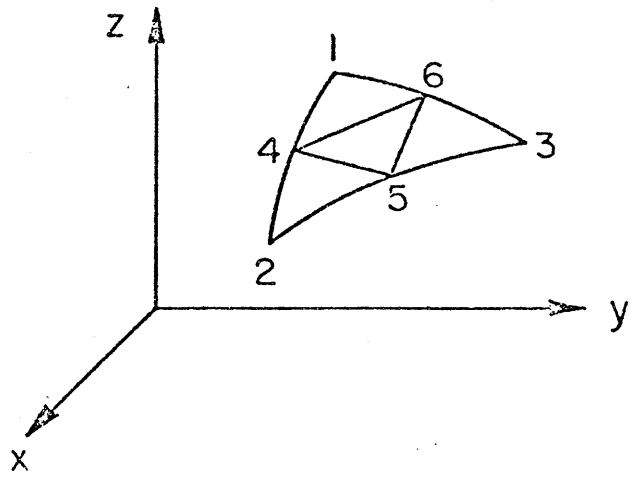

Fig. 2.7 Subregions for direct integration

2.6 SUCCESSIVE ELEMENT ITERATIVE SOLUTION

The integral finite-element discretization, in general results in a dense system of equations which is unfavourable in terms of both storage and computation. To handle economically problems of considerable size, an element-iterative scheme, which does not impose additional constraints and assumptions, is presented to supplement the finite-element integral technique. The method is derived from a method given by Shoamanesh and Shafai [34] used for solving loop current arrays. However, an essential difference in the two approaches is that, in [34], the interactions of variables which are not directly interconnected are not catered for. Hence the method may fail, for example, for cases where the effects of distant sources are dominant due to focusing effects. This constraint need not be imposed in the method described here. The approach is analogous, in the iterative sense, to the successive iterative procedures for the finite-difference mesh of a partial differential operator. As far as the matrix construction is concerned, the method is extended from the finite-element partial differential approach of treating each element individually in turn, although the procedure is much more complicated in the integral operator case.

Suppose the boundary is formed by n subregions each consisting of p elements with q total no. of nodes. The successive iterative scheme can be expressed implicitly as

$$\int_{S_k} K(s|s')\,\sigma^{(t+1)}(s')\,ds' = g(s) - \sum_{i=1}^{k-1} \int_{S_i} K(s|s')\,\sigma^{(t+1)}(s')\,ds' - \sum_{i=k+1}^{n} \int_{S_i} K(s|s')\,\sigma^{(t)}(s')\,ds' \quad (2.55)$$

where the bracketed superscript t denotes the iteration number and S_k refers to the kth subregion. The iterative process is initiated by assigning arbitrary values to all the unknowns. The Rayleigh-Ritz matrix equation corresponding to a single subregion is generated with the sources on all other subregions assumed to be known. The matrix equation is of the form

$$\begin{bmatrix} a_{11} & a_{12} & \cdots & a_{1q} \\ \vdots & & & \\ a_{q1} & \cdots & & a_{qq} \end{bmatrix} \begin{bmatrix} \sigma_1^{(t+1)} \\ \vdots \\ \sigma_q^{(t+1)} \end{bmatrix} = \begin{bmatrix} b_1 \\ \vdots \\ b_q \end{bmatrix} \tag{2.56}$$

The right-hand side vector is given by

$$\begin{bmatrix} b_1 \\ \vdots \\ b_q \end{bmatrix} = \begin{bmatrix} g_1 \\ \vdots \\ g_q \end{bmatrix} - \begin{bmatrix} b_{11} & b_{12} & \cdots & b_{1\ell} \\ \vdots & & & \\ b_{q1} & \cdots & & b_{q\ell} \end{bmatrix} \begin{bmatrix} h_1^{(t+1)} \\ \vdots \\ h_\ell^{(t+1)} \end{bmatrix} - \begin{bmatrix} c_{11} & c_{12} & \cdots & c_{1r} \\ \vdots & & & \\ c_{q1} & \cdots & & c_{qr} \end{bmatrix} \begin{bmatrix} f_1^{(t)} \\ \vdots \\ f_r^{(t)} \end{bmatrix} \tag{2.57}$$

where $\underline{h}$ is the vector of ℓ nodal values for the first (k-1) subregions and $\underline{f}$ is a vector of r nodal values for the remaining subregions (excluding the kth subregion) at the (t+1)th iteration. Equation (2.56) is a system of q equations to solve for the q unknown nodal values associated with the kth subregion. For each subregion solved, the current updated values are used immediately for subsequent computations. These "known" sources hence contributes to the right-hand side of the equation as if

one is solving a new problem with an augmented boundary condition. The process therefore involves solving a system of the size corresponds to the total number of unknowns within a single subregion. Large problems can therefore be handled at ease.

2.7 COMPUTER IMPLEMENTATION

The availability of efficient computing software plays an important role in the development and the subsequent applications of any numerical method. A FORTRAN program is coded for the above technique. It is general purpose in nature and is applicable to both scalar and vector fields.

The problem geometry and element identification, through vertex numbering, are specified by the input data. Only the vertices need to be numbered, but they may be numbered in any order. The appropriate number of nodes required for a degree N approximation is generated and numbered automatically from the scheme shown in Fig. 2.8 and Fig. 2.9

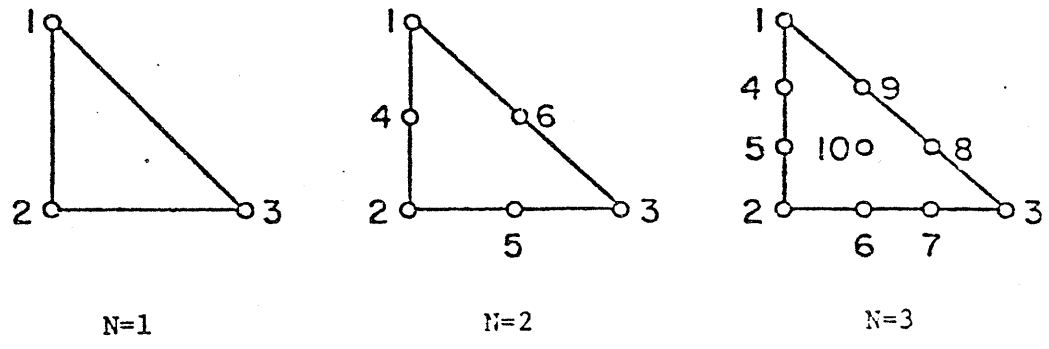

Fig. 2.8 Local numbering

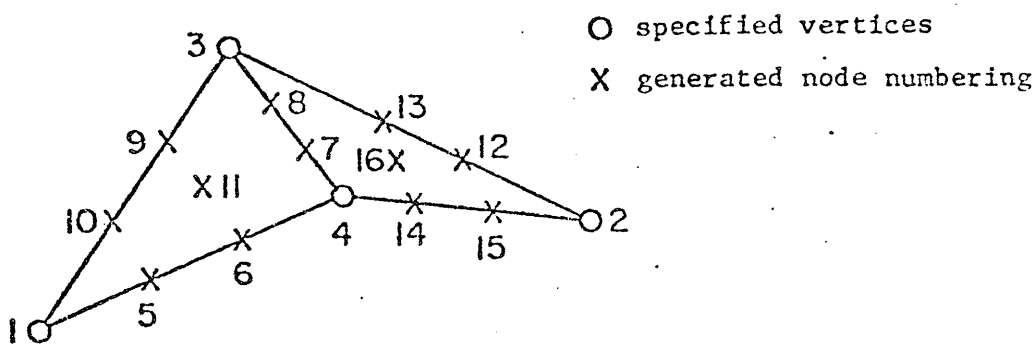

Fig. 2.9 Global numbering (N =3)
element 1: 1-4-3
element 2: 2-3-4

In addition to the high-order approximation of the geometry, an algorithmically important property is also provided by the parametric representation of the geometry described in Section 2.3. Since global elements are referenced to the local system, the integration over each and every arbitrarily shaped surface elements in the global system is performed over the two-dimensional simplex. This contributes to an essential algorithmic simplicity. Furthermore, only the set of Gaussian points associated with the simplex need to be generated — and this is done but once for all elements.

Insofar as the linear equation-solver is concerned, since the matrix S in equation (2.29), resulting from the discretization, is dense, standard Gaussian elimination [35] is used to solve the system of linear equations. With the computer zero at approximately 10^{-80} and infinity at approximately 10^{80}, a 40x40 matrix having elements with numerical values of the order 10^{-2} is likely to yield a vanishing determinant and hence

leads to a faulty termination of the solution process. Since multiplying each element of a NxN matrix [A] by a factor β results in the determinant being β^N times the determinant of [A], multiplying the elements of the matrix by an appropriate scaling factor will obviate the errors due to zero and/or infinity determinant.

2.8 CONCLUSION

In this chapter, a new, efficient and general algorithm — a generalization of the finite-element method for application to integral equations — has been presented for the solution of Fredholm equations arising in the boundary integral formulations of three-dimensional fields. This is a novel departure as the finite-element approximation method has traditionally been employed for partial differential equations.

The surface is modelled by triangular elements generated from an isoparametric mapping and the unknown function is approximated by polynomials. Analogous to the technique for partial differential equations, elements may be placed where desired for best representation. The high-order representation is expected to yield improved results as compared to the constant pulse approximation for the same number of variables. The matrix is constructed by considering one element at a time, in a fashion analogous to the partial differential finite-element technique. However, the procedure is more complicated here than for the partial differential equation case.

The matrix equation is dense which is characteristic of integral equation formulations. This is unfavourable as compared to the sparse equations of the partial differential approach. However, the integral

equation formulation having unknowns on the boundary only involves much fewer unknowns. The successive element iterative scheme described provides one way to obviate solving a large and dense matrix equation. Other approaches such as the frontal solution [47] may also be coupled to the integral finite-element method developed.

CHAPTER III

SOLUTION OF THREE-DIMENSIONAL ELECTROSTATIC FIELDS IN OPEN REGIONS

The need to solve a class of open-region electrostatic problems governed by the Laplace equation

$$-\nabla^2\phi = 0$$

arises frequently in, for example, the determination of parameters for open-wire transmission lines, microstrip discontinuities and certain antenna problems. For problems having locally homogeneous regions, boundary integral formulations, by which the unknown functions are defined only on the boundary and at interfaces rather than over the entire region, provides an efficient method of solution. The method has a clear advantage when the region is of infinite extent. In such cases, a problem involving an infinite region is replaced by one having a finite region of dimension one less than the original.

In this chapter, the finite-element integral approach described in Chapter II is presented to solve electrostatic field problems. Conducting boundaries having prescribed potentials are replaced with charge distributions in free space having the same potentials. Interfaces between regions of differing media are replaced by polarization charges. The equivalent source distribution formulation thus removes the requirement of finding special problem-dependent Green's functions and one needs to

be concerned only with the free-space Green's function.

The integral equation is discretized using the isoparametric finite element scheme previously described. The T-shaped conductor problem of Section 3.2, which is representative of a microstrip line discontinuity, demonstrates the improvement in convergence of the present scheme. The results are compared with those reported by McDonald, Friedman and Wexler [25] using pulse approximations. The prolate spheroid of Section 3.3 serves as an example of problems with arbitrary curved surfaces. Using a simple geometry, exact solution is available for comparison. Agreement was found with an accuracy far in excess of that which would be required in practical applications.

3.1 THE INTEGRAL APPROACH

Consider the scalar problem of finding the electrostatic field distribution governed by the Laplace equation

$$\nabla^2\phi(\bar{r}) = 0 \qquad \bar{r} \in R \tag{3.1}$$

and having prescribed potential on the boundary

$$\phi(s) = g(s) \qquad s \in S \tag{3.2}$$

It is well-known that solution to the problem is unique [38]. As far as the resulting field distribution is concerned, one is free to replace the boundary having prescribed potential by a source layer in free space which produces the given potential on the boundary and hence, on the whole, the required field distribution everywhere. The Dirichlet problem may then be posed in the form of an integral equation of the first kind

$$\frac{1}{\varepsilon_o} \int G(s|s')\ \sigma(s')\ ds' = g(s) \tag{3.3}$$

where G is the free-space Green's function

$$G(\bar{r}|\bar{r}') = \frac{1}{4\pi|\bar{r}-\bar{r}'|} \tag{3.4}$$

The Green's function given by (3.4) is symmetrical, that is, $G(\bar{r}|\bar{r}') = G(\bar{r}'|\bar{r})$, the integral operator in (3.3) is therefore self-adjoint. The unknown function $\sigma(s)$ is the equivalent single-layer source distribution to be determined. It is obvious that, for any charge distribution $\sigma(s)$, the potential given by

$$\phi(\bar{r}) = \frac{1}{\varepsilon_o} \int_S G(\bar{r}|s)\ \sigma(s)\ ds \tag{3.5}$$

satisfies the Laplace equation at all points due to the nature of the Green's function. However, (3.3) has a unique solution [39] and the required field distribution is produced by the set of charge distribution which satisfies the prescribed boundary potential.

From (2.7), the functional for the integral equation (3.3) is therefore

$$F = \frac{1}{\varepsilon_o} \int_S \sigma(s) \int_S G(s|s')\ \sigma(s')\ ds'ds - 2 \int_S \sigma(s)\ g(s)\ ds \tag{3.6}$$

Approximating $\sigma(s)$ by a linear combination of the basis functions $\underline{\alpha}(s)$, i.e., $\sigma(s) = \underline{\alpha}(s)^T \underline{\sigma}$, substituting into (3.6) and setting the first derivatives of F with respect to the variational parameters $\underline{\sigma}$ to zero yields

the system of equations

$$\frac{1}{\varepsilon_o} \int_S \underline{\alpha}(s) \int_S G(s|s') \, \underline{\alpha}^T(s') \, ds'ds \, \underline{\sigma} = \int_S \underline{\alpha}(s) \, g(s) \, ds \qquad (3.7)$$

Alternatively, the Galerkin method is to multiply both sides of (3.3) by the basis functions and integrating over S, i.e.,

$$\int_S \underline{\alpha}(s) \, [\frac{1}{\varepsilon_o} \int_S G(s|s') \, \sigma(s') \, ds'] \, ds = \int_S \underline{\alpha}(s) \, g(s) \, ds \qquad (3.8)$$

Substituting $\sigma(s) = \underline{\alpha}^T(s) \, \underline{\sigma}$, the system of equations given by (3.8) is

$$\frac{1}{\varepsilon_o} \int_S \underline{\alpha}(s) \int_S G(s|s') \, \underline{\alpha}^T(s') \, ds'ds \, \underline{\sigma} = \int_S \underline{\alpha}(s) \, g(s) \, ds \qquad (3.9)$$

Comparing (3.7) and (3.9), the system of equations derived from the variational approach is identical to that obtained by the Galerkin method.

3.2 THE T-SHAPED CONDUCTOR

We now consider a specific problem of finding the electrostatic field distribution of two parallel T-shaped conductors kept at constant potentials. The problem has been solved by McDonald, Friedman and Wexler [25] using a variational approach with pulse expansion functions.

The problem. Fig.3.1 shows two T-shaped conductors with the upper and the lower plates lying in the $z = 1$ and $z = -1$ planes, respectively. The potentials ϕ of the plates are kept at +1 and -1 volt, respectively.

Symmetry consideration allows the charge distribution to be sought in the positive quadrant, i.e., in the region $x \geq 0$, $y \geq 0$ and $z = 1$. From (3.3), the equation to be solved is

$$\frac{1}{\varepsilon_o} \int_S G(x,y,1|x',y',1)\ \sigma(x',y',1)\ ds = 1 \qquad (3.10)$$

where S is the portion of the plate in the positive quadrant at $z = 1$ shown in Fig. 3.2. $G(x,y,z|x',y',z')$ is the modified Green's function

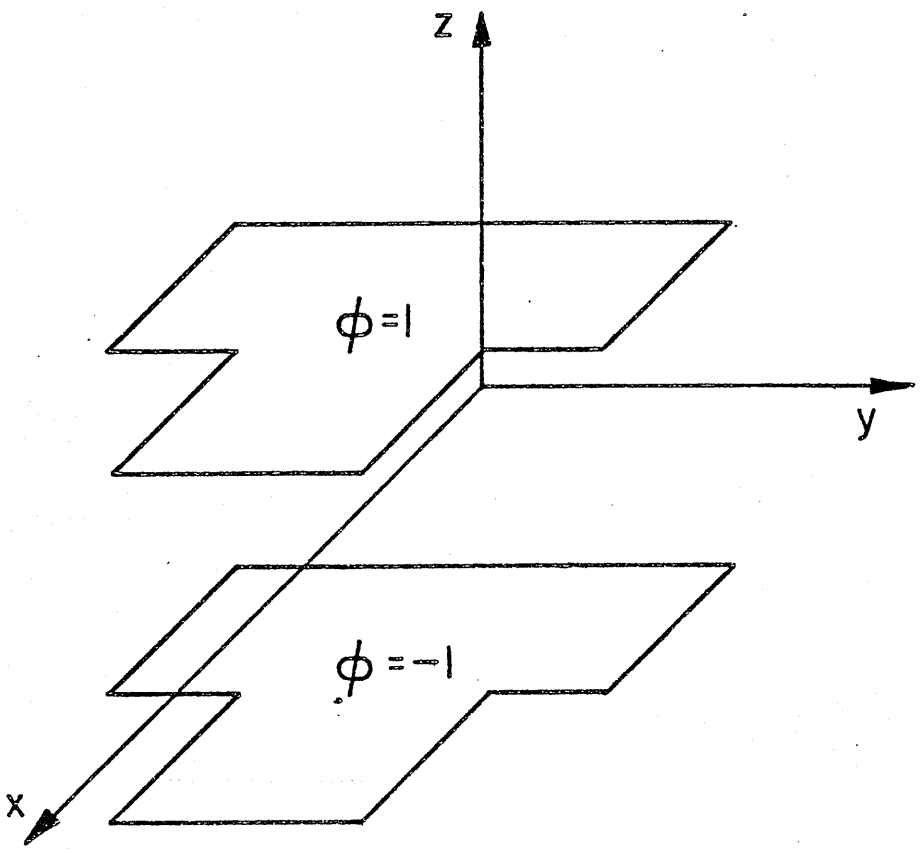

Fig. 3.1 The T-shaped conductor problem

given by

$$G(x,y,z|x',y',z') = \frac{1}{4\pi}\left\{\frac{1}{\sqrt{(x-x')^2+(y-y')^2+(z-z')^2}} + \frac{1}{\sqrt{(x-x')^2+(y+y')^2+(z-z')^2}}\right.$$

$$\left. - \frac{1}{\sqrt{(x-x')^2+(y-y')^2+(z+z')^2}} - \frac{1}{\sqrt{(x-x')^2+(y+y')^2+(z+z')^2}}\right\} \tag{3.11}$$

Finite-element discretization. The region is first divided into triangular subregions. Fig. 3.2 shows the finite-element model used. There are seven elements and eight vertex nodes. With a first-order approximation, the eight nodal values of $\sigma(s)$ are to be found. For a second-order approximation over each element, an additional node is placed at the midpoint of each and every side. There are a total number of 22 nodes in this case.

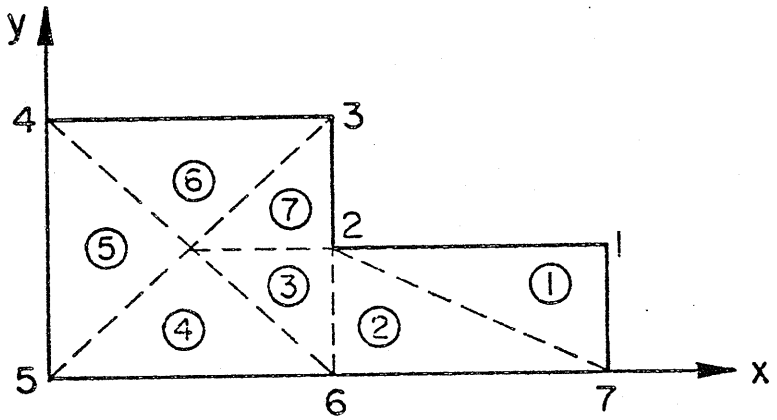

Fig. 3.2 A finite-element model of Fig. 3.1

The eight vertices are numbered in any order from 1 to 8 as shown in Fig. 3.2. These are the global nodal numbers. Elements are located by the global numbers of the three vertices, for example, element 5 is referred to by the sequence 4-5-8.

For the purpose of illustration, the case N = 1 is considered. From (3.7), the discretized system of equations for (3.10) pertaining to the model of Fig. 3.2 is given by

$$A\underline{\sigma} = \underline{b} \tag{3.12}$$

where A is a 8x8 matrix with the entry, a_{ij}, corresponding to the ith row and jth column given by

$$a_{ij} = \sum_{m\varepsilon V_i} \int_{S_m} \alpha_{p_{mi}}(s) \sum_{n\varepsilon V_j} \int_{S_n} G(s|s') \alpha_{p_{nj}}(s') \, ds'ds \tag{3.12a}$$

$\underline{\sigma}$ is the vector of unknown nodal values, $\underline{\sigma} = [\sigma_1,\sigma_2,\ldots,\sigma_8]^T$ and the ith entry of the 8x1 vector $\underline{b}$ is given by

$$b_i = \sum_{m\varepsilon V_i} \int_{S_m} \alpha_{p_{mi}}(s) \, ds$$

In (3.12a), V_k, k = 1,2,...,8, is the set of elements sharing node k as one of the vertices and p_{mi} is the local node number within element m of node i. Referring to Fig. 3.2, $V_1 = \{1\}$, $V_2 = \{1,2,3,7\}$, $V_3 = \{6,7\}$, etc.. Equation (3.12) is a system of 8 equations in the 8 unknown σ_i. The coefficient matrix is dense which is characteristic of integral equation formulations.

The finite-element technique allows the matrix generating process

to be carried out one element at a time. A contrast between the partial differential discretization and the integral discretization is that in the partial differential case, for each element, a MxM square matrix corresponding to the M nodal values of a single element is to be constructed. In the case of integral elements, because of the integral operation, all elements contribute to the entries of each and every row in generating the matrix equations for each individual element. These contributions from all other elements except the one under consideration can be included in the form of an augmented source term. Assuming, for the moment, the σ_{ij} terms of all other elements are known, the 3x3 matrix equation for the kth element is thus

$$\sum_{j=1}^{3} \sigma_{kj} \int_{S_k} \alpha_i(s) \int_{S_k} G(s|s') \alpha_j(s') \, ds'ds =$$

$$= \int_{S_k} \alpha_i(s) \, ds - \int_{S_k} \alpha_i(s) \sum_{\ell \neq k} \sum_{j=1}^{3} \sigma_{\ell j} \int_{S_\ell} G(s|s') \alpha_{p_{\ell j}}(s') \, ds'ds$$

$$i = 1,2,3 \qquad (3.13)$$

Now, since the sources are indeed not known, putting the unknown terms to the left- hand side of the equations, we have

$$\sum_{j=1}^{8} \int_{S_k} \alpha_i(s) \sum_{\ell \in V_j} \int_{S_\ell} G(s|s') \alpha_{p_{\ell j}}(s') \, ds'ds \, \sigma_j = \int_{S_k} \alpha_i(s) \, ds$$

$$i = 1,2,3 \qquad (3.14)$$

Since G is symmetric, interchanging the order of integration, (3.14) may

be rewritten as

$$\sum_{j=1}^{8} \sum_{\ell \in V_j} \int_{S_\ell} \alpha_{p_{j\ell}}(s) \int_{S_k} G(s|s')\, \alpha_i(s')\, ds'ds\, \sigma_j = \int_{S_k} \alpha_i(s)\, ds$$

$$i = 1,2,3 \qquad (3.15)$$

Therefore, for each element a set of three equations in 8 unknowns is constructed. These equations are constructed for each element in turn and are assembled to yield the global system of (3.12).

The matrix entries of (3.14) involve the evaluation of the integral

$$\int_S \alpha_p(s) \int_S G(s|s')\, \alpha_q(s')\, ds'ds \qquad (3.16)$$

From (2.48), the integral (3.16) is computed by first rewriting it as

$$I = I_1 + I_2 \qquad (3.17)$$

where

$$I_1 = \int_S \alpha_p(s) \int_S [G(s|s')\alpha_q(s') - G_s(s|s')\alpha_q(s)]\, ds'ds \qquad (3.18)$$

and

$$I_2 = \int_S \alpha_p(s)\, \alpha_q(s) \int_S G_s(s|s')\, ds'ds \qquad (3.19)$$

G_s contains the singular function

$$G_s(s|s') = \frac{1}{\sqrt{(x-x')^2+(y-y')^2+(z-z')^2}} \tag{3.20}$$

The first term of (3.17) is regular and is computed numerically by a double application of Gaussian quadrature [33] over the simplex as detailed in Section 2.5. The integrated value is

$$I_1 = \sum_{i=1}^{n} \sum_{j=1}^{n} a_i a_j \, \alpha_p(s_i) \, h(s_i,s_j) \tag{3.21}$$

where

$$h(s_i,s_j) = [G(s_i|s_j) \, \alpha_q(s_j) - G_s(s_i|s_j) \, \alpha_q(s_i)] \tag{3.22}$$

The closed-form expression for the inner integral of I_2 is given by (2.53). The outer integral is then computed directly using Gaussian quadrature.

Numerical results. The results obtained are summarized in Table 3.1. For ease of comparison, the pulse-function variational solution is also included.

The pulse solution was obtained with the unknown function being approximated by constants over rectangles shown in Fig. 3.3 for the positive-quadrant plate. With the pulse solution using 24 variables, the computed capacitance is 125.6 pf whereas the finite-element model using first-order approximation with 8 unknown variables, a comparable value of 124.23 pf is obtained. Roughly, 24 and 54 pulse variables

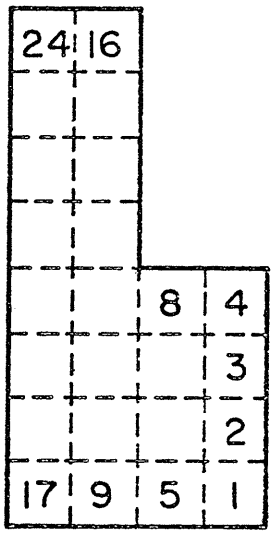

Fig. 3.3 Constant-pulse approximation for the T-plate problem

appear to correspond to the accuracy obtained by 8 and 22 variables, respectively, the latter involving smooth polynomials. The comparison made here is slightly in favour of the finite-element approach due to the fact that a higher capacitance value in the pulse case is compared to that of the finite-element case. In a subsequent example, the finite-element solution is compared to the exact solution.

As far as the amount of computation involved is concerned, in generating the matrix equations, the pulse solution using 24 variables requires the evaluation of 300 double surface integrals having taken into consideration the symmetries of the matrix. On the other hand, by a close examination of (3.15), the column entries in each row corresponding to one element can be generated by performing a double integration but once. A considerable saving results in not having to compute

TABLE 3.1

The T-plate Problem

Constant pulse over rectangle			Triangular finite element with higher order approximations			
No. of pulses	Capacitance (pf)	Potential ϕ (2,3,2)	Degree of approximation	No. of nodes	Capacitance (pf)	Potential ϕ (2,3,2)
6	119.4	.1968				
24	125.6	.2064	1	8	124.23	.20564
54	127.8	.2102	2	22	127.43	.21138

the double integrals of (3.15) term by term. This is the algorithm used for constructing the matrix equation in the integral finite-element package developed. Therefore, for a solution of comparable accuracy, the finite-element model with 7 elements and 8 variables requires the evaluation of 147 double surface integrals. The finite-element approach is, therefore, superior to the pulse approximation in terms of computing effort.

Notice also that by means of boundary integral formulations, simply by solving a system of 8 equations, the solution to the three-dimensional

problem is obtained. Moreover, the solution is obtained in an infinite space by performing the integration (3.5).

3.3 AN ELLIPSOID

As an example of problems with arbitrary curved surfaces, the integral finite-element method is applied to the determination of the capacitance and the field distribution of a prolate spheroid. For this problem, exact solution, derived from the method of separation of variables to the partial differential formulation, is available for comparison and serves to justify the validity of the technique and the computer implementation.

The problem. Consider a three-dimensional ellipsoidal conducting body with principal semi-axes a = 2, b = c = 1 and kept at a constant potential $\phi = 1$. Fig. 3.4 shows the configuration.

Making use of symmetry, the source distribution is sought over one-sixteenth of the ellipsoidal surface. From (3.3), the equation to be solved is

$$\frac{1}{\varepsilon_o} \int_S G(x,y,z|x',y',z')\ \sigma(x',y',z')\ ds = 1 \qquad (3.23)$$

where the domain of integration S is over one-sixteenth of the total surface and G is the modified free-space Green's function given by

$$G(x,y,z|x',y',z') = \frac{1}{4\pi} \left\{ \frac{1}{\sqrt{(x\pm x')^2+(y\pm y')^2+(z\pm z')^2}} + \frac{1}{\sqrt{(x\pm x')^2+(y\pm z')^2+(z\pm y')^2}} \right\}$$

(3.24)

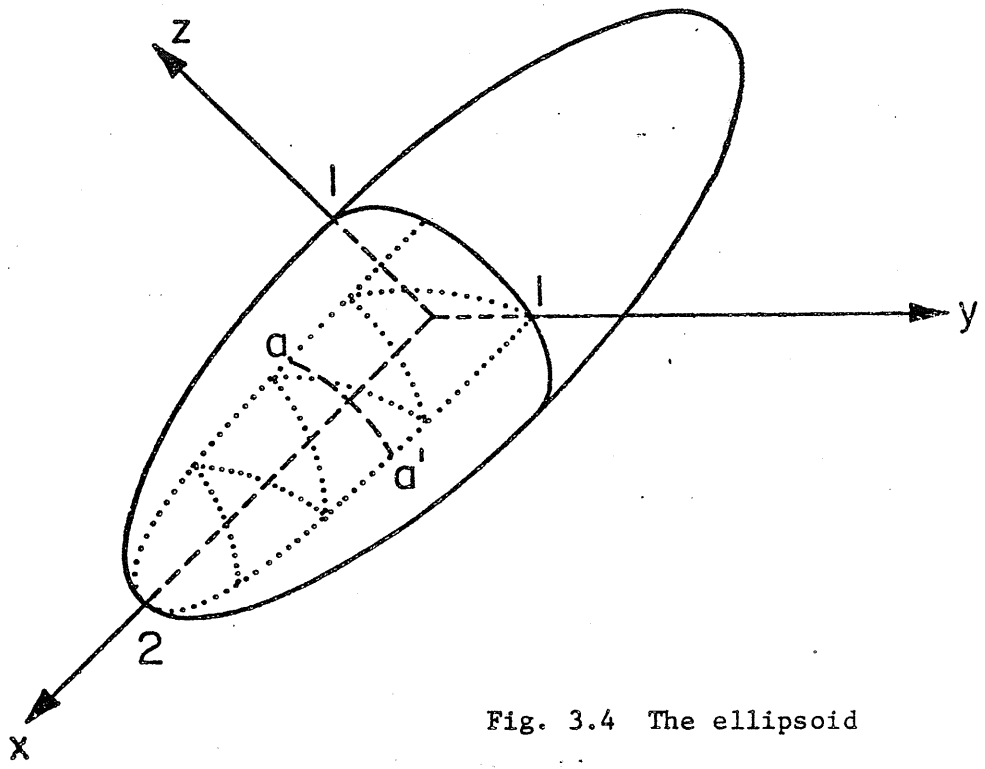

Fig. 3.4 The ellipsoid

Each term on the right-hand side of (3.24) consists of eight terms formed from the eight possible combinations of the plus and minus signs associated with the x', y' and z'.

Finite-element solution. The finite-element model used is shown by the dotted lines in Fig. 3.4. Seven elements were used over one-sixteenth of the surface. It is well-recognised that an accurate definition of boundary shapes is one of the essential factors in obtaining accurate solutions. In contrast to the common procedure of using a large number of piecewise flat surfaces to model curved surfaces, the ellipsoidal surface is approximated by curved surfaces generated from the isoparametric mapping described in Section 2.4. Table 3.2 gives a measure of the closeness of the generated surface to the actual surface. For an exact mapping,

the column r takes the value 0.8992, being the radius of the cross-section of the ellipsoid at x = 0.875. The reduction in the modelling error from the linear model to the curved surface model is obvious.

The results presented in Table 3.3 give a clear indication of the improvement in the accuracy of the solution obtained by using second-order elements as compared to first-order elements. Here, by solving a system of 22 equations corresponding to the second-order approximation, the field at any point in an infinite space may be computed directly from the integral (3.5). The exact value of the capacitance in Table 3.3 is evaluated from the expression [40]

$$C = \{8\pi\varepsilon_0(a^2-b^2)^{\frac{1}{2}}\}/\log\{\frac{a+(a^2-b^2)^{\frac{1}{2}}}{a-(a^2-b^2)^{\frac{1}{2}}}\} \tag{3.25}$$

and the potential ϕ at (x,y,z) is given by

$$\phi = \frac{e}{8\pi\varepsilon_0(a^2-b^2)^{\frac{1}{2}}} \log \frac{(a^2+u)^{\frac{1}{2}} + (a^2-b^2)^{\frac{1}{2}}}{(a^2+u)^{\frac{1}{2}} - (a^2-b^2)^{\frac{1}{2}}} \tag{3.26}$$

where e is the charge on the ellipsoid and u is the ellipsoidal coordinate defined by

$$\frac{x^2}{a^2+u} + \frac{y^2}{b^2+u} + \frac{z^2}{c^2+u} = 1 \qquad (-c^2<u,\ a>b>c). \tag{3.27}$$

An iterative approach. We have also solved the problem using the element iterative scheme described in Section 2.7. The same model shown in Fig. 3.4 used in the direct solution approach is used here. The region is divided into seven subregions each consisting of a single element.

TABLE 3.2

Mapping at $x = 0.875$ for
the ellipsoid $x^2/4+y^2+z^2 = 1$
Exact $r = \sqrt{1-x^2/4} = 0.8992$

y	z	$r = \sqrt{y^2+z^2}$
0.8990	0.0000	0.8990
0.8670	0.2343	0.8981
0.8075	0.3954	0.8991
0.7509	0.4957	0.8998
0.6779	0.5906	0.8990

TABLE 3.3

Ellipsoid - using linear triangular and curved elements

			Capacitance (exact = 146.33pf)		Potential $\phi(0,2,0)$ (exact = 0.59484)	
No. of elements	Degree of approximation	No. of nodes	Linear triangular elements	Isoparametric elements	Linear triangular elements	Isoparametric elements
7	1	9	138.80	138.80	0.56905	0.56905
7	2	22	139.13	145.72	0.57021	0.59355

The iterative process is initiated by suppressing the sources on all subregions except subregion 1. For this subregion, a set of M equations, with M being related to the degree of approximation N by $M = (N+1)(N+2)/2$, may now be constructed as

$$\begin{bmatrix} \int_{S_1}\alpha_1(s)\int_{S_1}G(s|s')\alpha_1(s')ds'ds & \cdots & \int_{S_1}\alpha_1(s)\int_{S_1}G(s|s')\alpha_M(s')ds'ds \\ \vdots & & \\ \int_{S_1}\alpha_M(s)\int_{S_1}G(s|s')\alpha_1(s')ds'ds & \cdots & \int_{S_1}\alpha_M(s)\int_{S_1}G(s|s')\alpha_M(s')ds'ds \end{bmatrix} \begin{bmatrix} \sigma_{11}^{(1)} \\ \vdots \\ \sigma_{1M}^{(1)} \end{bmatrix} = \begin{bmatrix} \int_S \alpha_1(s)ds \\ \vdots \\ \int_S \alpha_M(s)ds \end{bmatrix} \tag{3.28}$$

In (3.28), the entries to the right-hand side vector $\underline{b}$ are due to sources on subregion 1 only, since all other sources are assumed to be zero. Equation (3.28) is solved for the nodal values of subregion 1. These updated approximations are used immediately in the form of augmented sources in obtaining solutions for other subregions. Therefore, for the kth subregion, a system of equations analogous to (3.28) but with the vector $\underline{b}$ amended as

$$\begin{bmatrix} \int_{S_k}\alpha_1(s)ds - \int_{S_k}\alpha_1(s)\sum_{i=1}^{k-1}\int_{S_i}G(s|s')\,\sigma^{(1)}(s')\,ds'ds \\ \vdots \\ \int_{S_k}\alpha_M(s)ds - \int_{S_k}\alpha_M(s)\sum_{i=1}^{k-1}\int_{S_i}G(s|s')\,\sigma^{(1)}(s')\,ds'ds \end{bmatrix} \tag{3.29}$$

is constructed. In (3.29), the second summation is up to the (k-1) subregion as the sources on remaining subregions are not computed yet. Each time, an updating approximation is obtained for the subregion under consideration. The iterative process of (2.55) is repeated until the difference in solution between two successive iterations is smaller than some prespecified tolerance.

Table 3.4 shows the convergence characteristic for the first-order approximate solution. A monotone convergence to the solution is observed. A value of 138.43 pf for the capacitance is obtained in 6 iterations as compared to 138.80 pf from the direct solution scheme, the former involving solution of matrix equations only of order 3.

Point-matching and variational comparison. Instead of generating the discretized equations from the energy functional together with the Rayleigh-Ritz procedure, the continuum problem may be discretized by writing equation (3.23) directly at the n nodal points to obtain a system of n equations, while retaining the high-order approximations of the function and the geometry as in the finite-element method. This discretization procedure of constraining the equation at points is known as the point-matching method. It is a special case of the moment method [14] with delta function testing.

Constraining the equation at n nodal points, the point-matching equations for (3.23) is therefore given by

$$\begin{bmatrix} \sum_{i\in V_1} \int_{S_i} G(s_1|s)\alpha_{i1}(s)\,ds & \cdots & \sum_{i\in V_n} \int_{S_i} G(s_1|s)\alpha_{in}(s)\,ds \\ \vdots & & \\ \sum_{i\in V_1} \int_{S_i} G(S_n|s)\alpha_{i1}(s)\,ds & \cdots & \sum_{i\in V_n} \int_{S_i} G(s_n|s)\alpha_{in}(s)\,ds \end{bmatrix} \begin{bmatrix} \sigma_1 \\ \vdots \\ \sigma_n \end{bmatrix} = \varepsilon_o \begin{bmatrix} 1 \\ \vdots \\ 1 \end{bmatrix} \tag{3.30}$$

where s_1, s_2, ..., s_n are the node points where equality is imposed on the continuum equation. The right-hand side vector of (3.30) is simply a vector of constant 1 times the scalar ε_o because the surface is kept at unit potential. Note that (3.30) is not a symmetric system.

Fig. 3.5 shows a comparison of solution errors using the point-matching and the variational methods. The variational approach requires a smaller number of variables than would the point-matching method for the same accuracy. However, the variational approach involves the expensive double integrations as compared to single integrations required by the point-matching method in the evaluation of matrix entries. Moreover, the variational matrix is generated on an element basis. The amount of computation involved therefore is also a function of the subdivision of the structure. A rigorous comparison of the computation cost would not be representative. Nevertheless, it is undoubtly that for a given number of variables, the variational approach is more expensive than the point-

TABLE 3.4

Successive element iterative solution --
The ellipsoid with N=1.
Direct solution value = 138.80pF

Iteration No.	1	2	3	4	5	6
Capacitance	168.80	153.91	145.70	141.32	139.24	138.43

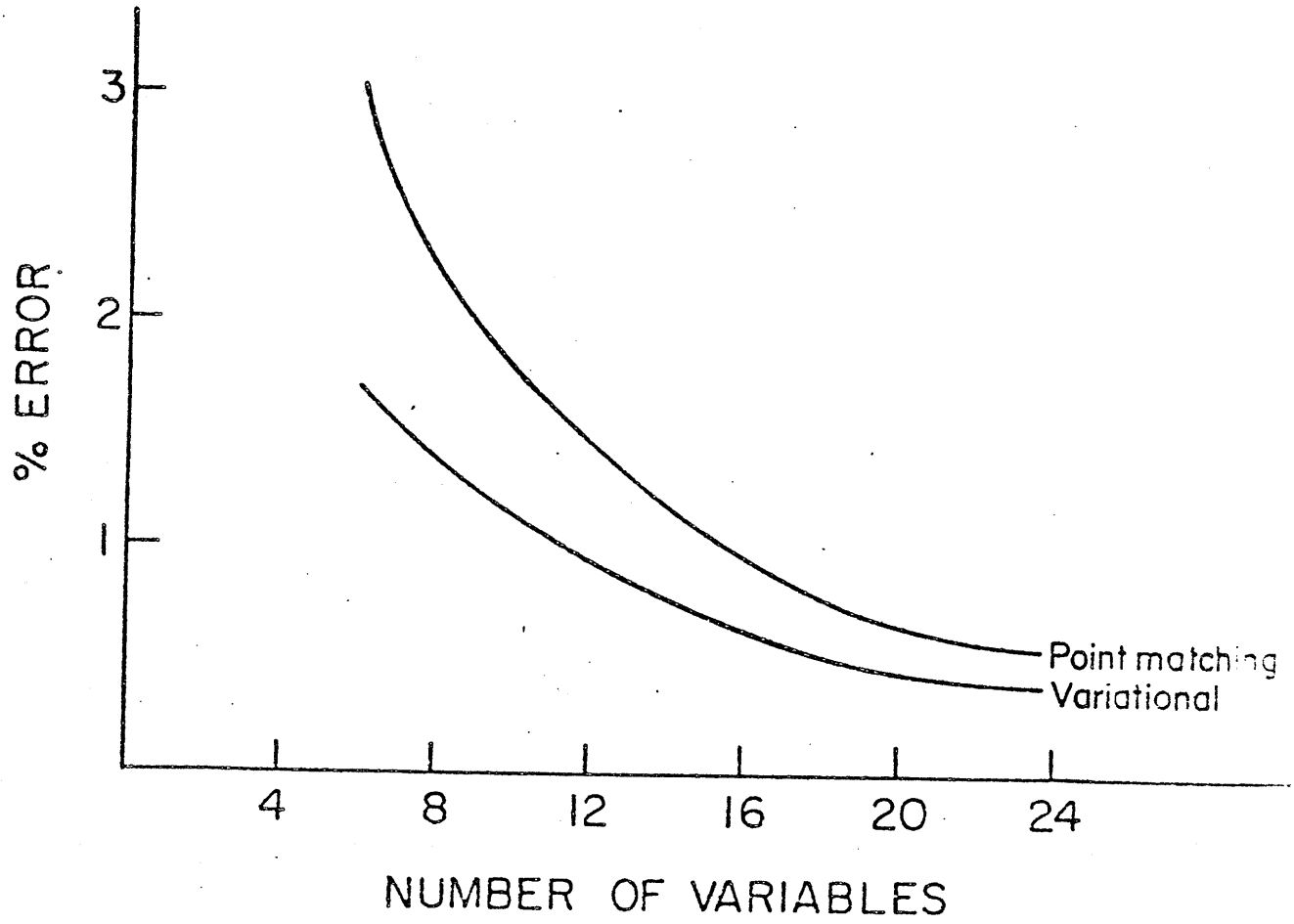

Fig. 3.5 Variational and point-matching comparison

matching method. On the other hand, for the same variables, the variational approach yields better result. Moreover, with the former, one is guaranteed of convergence [13] whereas such convergence proof lacks in the point-matching method. There is, therefore, a trade-off between the relative merits as mentioned of the two approaches.

CHAPTER IV

SOLUTION OF MAGNETOSTATIC FIELDS

The technique described in Chapter II provides an efficient, algorithmically simple and practical method of solving three-dimensional problems with arbitrary geometries. In this chapter, the method is illustrated to the solution of magnetostatic fields.

Various integral equation methods for the calculation of magnetic fields have been reported by Trowbridge [41]. As pointed out in [41], the magnetization integral equation method involves the vector magnetization as the unknown quantity defined over the entire volume of permeable materials. Thus, numerical discretization involving three components of a vector quantity is performed over the entire region. The scalar formulation, on the other hand, overcomes the disadvantage of solving three components of a vector quantity. Furthermore, with boundary formulations, only boundaries of regions of different permeabilities have to be divided into elements. A boundary integral formulation in magnetic scalar potential is presented in [41], in which both the potential ϕ and its normal derivative on boundary surfaces only are treated as independent variables and are interpolated independently. This formulation of having both ϕ and its normal derivative as unknowns is parallel to the generally referred to two-field formulation in

elasticity where both the displacement and stress fields are taken as variables [42]. Alternatively, by combining the interface constraint equations and the governing integral equation derived from the Green's theorem, a boundary integral equation in the magnetic scalar potential ϕ alone is derived. This single-field formulation reduces the number of variables and results in computational saving. The equation is derived in Section 4.2. An integration scheme is described in Section 4.3 to compute the free-space field due to current sources in conductors of arbitrary configurations. In Section 4.4, the finite-element method is applied to obtain an approximate solution of the boundary integral equation for the problem of a permeable prolate spheroid in an uniform applied field. The field at any point in space is then calculated from the boundary solution. It will be shown that the expression for computing ϕ values in the region exterior to the permeable body is numerically unstable. Nevertheless, the single-field formulation reduces the number of variables and is a preferable formulation if only the field in the permeable region is of interest. In Section 4.5, a magnet problem is solved.

4.1 BASIC FIELD EQUATIONS

The fundamental expressions which govern the magnetostatic field distribution are

$$\nabla \times \bar{H} = \bar{J} \tag{4.1}$$

$$\nabla \cdot \bar{B} = 0 \tag{4.2}$$

where $\bar{H}$ is the magnetic field intensity, $\bar{J}$ the current density and $\bar{B}$ is the magnetic flux density. In a linear media, $\bar{B}$ and $\bar{H}$ are related by

$$\bar{B} = \mu \bar{H} \tag{4.3}$$

where μ is the permeability of the magnetic material.

Expressing the field $\bar{H}$ at any point as the sum of two field components, $\bar{H}_c$ and $\bar{H}_m$

$$\bar{H} = \bar{H}_c + \bar{H}_m \tag{4.4}$$

with $\bar{H}_c$ being the field due to current sources $\bar{J}$ and $\bar{H}_m$ the field due to polarization effects [41]. Equation (4.1) therefore yields

$$\nabla \times \bar{H}_c = \bar{J} \tag{4.5}$$

and

$$\nabla \times \bar{H}_m = 0 \tag{4.6}$$

Using the Biot-Savart law, the field $\bar{H}_c$ is given by

$$\bar{H}_c = \frac{1}{4\pi} \int_V \frac{\bar{J} \times (\bar{r}-\bar{r}')}{|\bar{r}-\bar{r}'|^3} \, dv \tag{4.7}$$

where the integration is performed over the entire region where current source exists.

From (4.6), the magnetization component $\bar{H}_m$ can therefore be expressed as the gradient of a scalar function

$$\bar{H}_m = -\nabla\phi \tag{4.8}$$

Substituting (4.3), (4.4) and (4.8) into (4.2), the poisson equation for the scalar field is

$$\nabla\cdot(\mu\nabla\phi) = \nabla\cdot(\mu\bar{H}_c) \tag{4.9}$$

At the interface between regions of differing materials, the flux continuity condition holds, i.e.,

$$B_{n1} = B_{n2} \tag{4.10}$$

where n is the normal at the interface and subscripts 1 and 2 denote regions 1 and 2, respectively. From (4.3), (4.4) and (4.8), (4.10) — in terms of scalar potential ϕ — is

$$\mu_1 \frac{\partial\phi(s)}{\partial n_1} - \mu_2 \frac{\partial\phi(s)}{\partial n_2} = (\mu_1-\mu_2)\, H_{cn}(s) \tag{4.11}$$

where H_{cn} denotes the normal component of the source field $\bar{H}_c$ at S.

If the permeability of the region is constant, the governing differential equation reduces to the Laplace equation

$$\nabla^2\phi = 0 \tag{4.12}$$

since $\nabla\cdot\bar{H}_c = 0$.

4.2 DERIVATION OF THE BOUNDARY INTEGRAL EQUATION

Consider the problem depicted in Fig. 4.1. The magnetic field in the presence of a permeable body placed in an external field $\bar{H}_c$ due to current sources of density $\bar{J}$ is to be determined.

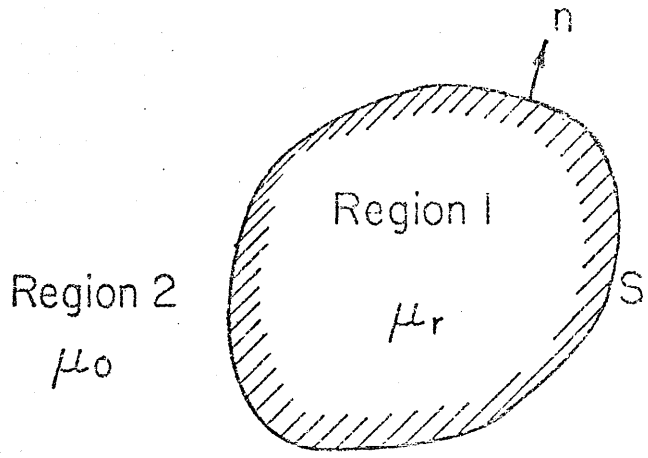

Fig. 4.1 An interface problem

Denoting by ψ and ϕ two functions continuous in R together with first and second derivatives, the Green's second theorem is stated as

$$\int_R [\psi(\bar{r})\ \nabla^2\phi(\bar{r}) - \phi(\bar{r})\ \nabla^2\psi(\bar{r})]\ d\Omega$$

$$= \int_S [\psi(s)\ \frac{\partial\phi(s)}{\partial n} - \phi(s)\ \frac{\partial\psi(s)}{\partial n}]\ ds \qquad (4.13)$$

where n is the outward normal at the surface S.

Taking ψ to be the Green's function $G(\bar{r}|\bar{r}')$ defined by

$$\nabla^2 G(\bar{r}|\bar{r}') = -\delta(\bar{r}-\bar{r}') \tag{4.14}$$

for a harmonic ϕ, the first term of the left-hand side integral vanishes and (4.13) yields

$$\int_R -\phi(\bar{r}')\ \nabla^2 G(\bar{r}|\bar{r}')\ d\Omega = \int_S [G(\bar{r}|s)\ \frac{\partial\phi(s)}{\partial n} - \phi(s)\ \frac{\partial G}{\partial n}\ (\bar{r}|s)]\ ds \tag{4.15}$$

In three-dimensional space, $G(\bar{r}|\bar{r}')$ is given by

$$G(\bar{r}|\bar{r}') = \frac{1}{4\pi|\bar{r}-\bar{r}'|} \tag{4.16}$$

In [41], both the potential ϕ and its normal derivatives $\frac{\partial\phi}{\partial n}$ on S are treated as independent variables. Thus, at the interface between regions of differing permeabilities, both ϕ and $\frac{\partial\phi}{\partial n}$ are unknowns. The discretized system of equations derived from (4.15) is therefore underdetermined. Additional set of equations are introduced from interface conditions.

Now, consider an observation point $\bar{r}$ in R_2. Applying Green's theorem to R_2, we have

$$\phi_2(\bar{r}) = -\int_S [G(\bar{r}|s)\ \frac{\partial\phi_2(s)}{\partial n} - \phi_2(s)\ \frac{\partial G}{\partial n}\ (\bar{r}|s)]\ ds \tag{4.17}$$

The minus sign associated with the right-hand side integral in (4.17) is introduced due to the normal being defined as the inward normal to R_2. The surface integral is performed over the interface between R_1 and R_2.

The integral for the boundary at infinity vanishes [4].

Similarly, applying Green's theorem to R_1 and considering an observation point $\bar{r}$ in R_1 yields

$$\phi_1(\bar{r}) = \int_S [G(\bar{r}|s) \frac{\partial \phi_1(s)}{\partial n} - \phi(s) \frac{\partial G}{\partial n}(\bar{r}|s)] \, ds \tag{4.18}$$

We now examine the integrals in (4.17) and (4.18). The first integral of (4.17) and (4.18) has the form of the single layer potential which is continuous as $\bar{r}$ crosses the boundary surface S [4]. The second integral, resembling the double layer potential, is discontinuous at S. Letting

$$f(\bar{r}) = \frac{1}{4\pi} \int_S \beta(s) \frac{\partial}{\partial n} \left(\frac{1}{|\bar{r}-s|}\right) ds \tag{4.19}$$

the discontinuity as $\bar{r}$ approaches p from either side of the surface (Fig. 4.2) is given by [4]

$$f_+(p) = \lim_{\bar{r} \to p_+} f(\bar{r}) = \frac{\beta(p)}{2} + \frac{1}{4\pi} \int_S \beta(s) \frac{\partial}{\partial n} \left(\frac{1}{|p-s|}\right) ds \tag{4.20}$$

$$f_-(p) = \lim_{\bar{r} \to p_-} f(\bar{r}) = -\frac{\beta(p)}{2} + \frac{1}{4\pi} \int_S \beta(s) \frac{\partial}{\partial n} \left(\frac{1}{|p-s|}\right) ds \tag{4.21}$$

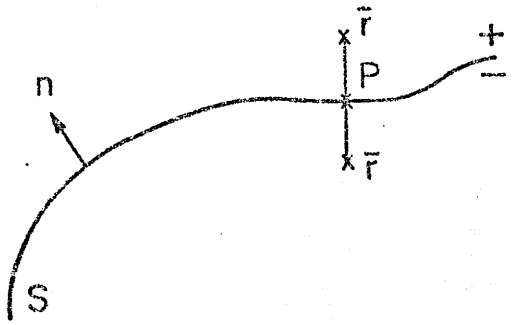

Fig. 4.2
Notation for boundary limits of eqns. (4.20) and (4.21)

Substituting (4.20) into the second integral of (4.17) and rearranging terms, we have

$$\frac{\phi_2(s)}{2} = -\int_S G(s|s') \frac{\partial \phi_2(s')}{\partial n} ds' - \int_S \phi_2(s') \frac{\partial G}{\partial n}(s|s') ds' \quad (4.22)$$

Similarly, from (4.21), as $\bar{r}$ approaches S, (4.18) yields

$$\frac{\phi_1(s)}{2} = \int_S G(s|s') \frac{\partial \phi_1(s')}{\partial n} ds' - \int_S \phi_1(s') \frac{\partial G}{\partial n}(s|s') ds' \quad (4.23)$$

Adding (4.22) to (4.23) multiplied by μ_r, we have

$$\begin{aligned} \frac{1}{2}(\mu_r \phi_1(s) + \phi_2(s)) &= \int_S G(s|s') \left(\mu_r \frac{\partial \phi_1(s')}{\partial n} - \frac{\partial \phi_2(s')}{\partial n}\right) ds' \\ &= \int_S [\mu_r \phi_1(s') - \phi_2(s')] \frac{\partial G}{\partial n}(s|s') ds' \end{aligned} \quad (4.24)$$

Imposing the continuity conditions

$$\begin{aligned} &\phi_1(s) = \phi_2(s) \\ &\mu_r \frac{\partial \phi_1(s)}{\partial n} - \frac{\partial \phi_2(s)}{\partial n} = (\mu_r - 1) H_{cn}(s) , \end{aligned} \quad (4.25)$$

(4.24) yields

$$\begin{aligned} &\frac{\mu_r + 1}{2} \phi(s) + (\mu_r - 1) \int_S \phi(s') \frac{\partial G}{\partial n}(s|s') ds' \\ &\qquad = (\mu_r - 1) \int_S G(s|s') H_{cn}(s') ds' \end{aligned} \quad (4.26)$$

Equation (4.26) is an integral equation of the second kind in ϕ. The field component $\bar{H}_c$ from the current sources, i.e., the imposed field, enters into the expression as the known right-hand side term.

Now, for an observation point $\bar{r}$ in R_1, the Green's theorem applied to region R_2 gives the relation

$$\int_S [G(\bar{r}|s) \frac{\partial \phi_2}{\partial n} - \phi_2(s) \frac{\partial G}{\partial n} (\bar{r}|s)] \, ds = 0 \tag{4.27}$$

From (4.18) and (4.27) together with the continuity conditions (4.25), the field at an observation point $\bar{r}$ in R_1 due to the polarization effect is given by

$$\phi_1(\bar{r}) = \frac{(\mu_r - 1)}{\mu_r} \int_S [G(\bar{r}|s) H_{cn}(s) - \phi_1(s) \frac{\partial G}{\partial n} (\bar{r}|s)] \, ds \tag{4.28}$$

Similarly, for an observation point $\bar{r}$ in R_2, equation (4.17) together with the continuity conditions and the relation obtained by applying the Green's theorem to R_1

$$\int_S [G(\bar{r}|s) \frac{\partial \phi_1(s)}{\partial n} - \phi_1(s) \frac{\partial G}{\partial n} (\bar{r}|s)] \, ds = 0 \tag{4.29}$$

give

$$\phi_2(\bar{r}) = (\mu_r - 1) \int_S [G(\bar{r}|s) H_{cn}(s) - \phi_2(s) \frac{\partial G}{\partial n} (\bar{r}|s)] \, ds \tag{4.30}$$

The gradient of ϕ gives the magnetization component $\bar{H}_m$. The resultant field is then obtained as the vector sum of the two field components, $\bar{H}_c$ and $\bar{H}_m$.

4.3 VOLUME INTEGRATION FOR SOURCE FIELD

The $\bar{H}_c$ field in the right-hand side of (4.26) due to current source of density $\bar{J}$ is obtained from the Biot-Savart law

$$\bar{H}_c = \frac{1}{4\pi} \int_V \frac{\bar{J} \times (\bar{r}-\bar{r}')}{|\bar{r}-\bar{r}'|^3} \, dv \tag{4.31}$$

where the integration is to be performed over the entire region where current exists. As noted from (4.26), the normal components of $\bar{H}_c$ are to be determined at quadrature points in the region of integration. The integration of (4.31) is to be carried out numerically whenever the closed-form expression is not possible.

An integration scheme is described to evaluate the volume integration (4.31). Analogous to the algorithm described in Chapter II for computing the surface integrals in the finite-element method, the volume integration is performed in local coordinates. This provides algorithmic generality of the entire procedure and also facilitates a full automation of the algorithm.

Two types of volume elements are described, the cube and the prism. Consider first the cube element with the local coordinate system u-v-w as shown in Fig. 4.3.

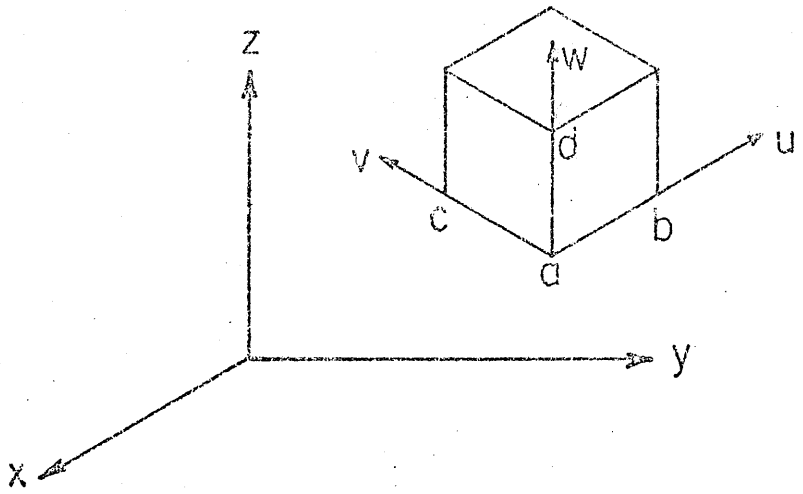

Fig. 4.3 The cube element

The local and global coordinates are therefore related by

$$u = \{(x-x_a)(x_b-x_a) + (y-y_a)(y_b-y_a) + (z-z_a)(z_b-z_a)\}/u_b$$

$$v = \{(x-x_a)(x_c-x_a) + (y-y_a)(y_c-y_a) + (z-z_a)(z_c-z_a)\}/v_c \qquad (4.32)$$

$$w = \{(x-x_a)(x_d-x_a) + (y-y_a)(y_d-y_a) + (z-z_a)(z_d-z_a)\}/w_d$$

The volume integral

$$I_1 = \int_V f(x,y,z)\ dv \qquad (4.33)$$

is therefore given by

$$I_1 = \int_{w_a}^{w_d} \int_{v_a}^{v_c} \int_{u_a}^{u_b} f(u,v,w)\ dudvdw \qquad (4.34)$$

By the simple transformation

$$u = u_a + (u_b - u_a)u'$$
$$v = v_a + (v_c - v_a)v' \qquad (4.35)$$
$$w = w_a + (w_d - w_a)w'$$

the integral (4.34) is obtained as

$$I_1 = \int_0^1 \int_0^1 \int_0^1 f(u,v,w) \; |J| \; du'dv'dw' \qquad (4.36)$$

where J is the Jacobian of transformation given by

$$J = (u_b - u_a)(v_c - v_a)(w_d - w_a) \qquad (4.37)$$

A triple application of numerical quadratures in one variable,

$$\int_0^1 f(x) \; dx = \sum_{i=1}^{n} a_i f(x_i) \qquad (4.38)$$

yields, for (4.36),

$$\int_0^1 \int_0^1 \int_0^1 f(u,v,w) \; |J| \; du'dv'dw' = \sum_{i=1}^{n} \sum_{j=1}^{n} \sum_{k=1}^{n} a_i a_j a_k \; |J| \; f(u_i', v_j', w_k') \qquad (4.39)$$

where the coefficients a_i are the weights at u_i and (u_i', v_j', w_k') are quadrature points in the unit cube. These points need be generated but once for all volume integrations to be evaluated.

Consider now the prism element which provides a basic element for

integration over arbitrary regions having uniform cross-section. A local coordinate system u-v-w is defined as shown in Fig. 4.4. The u-v plane is in the plane of the cross-section.

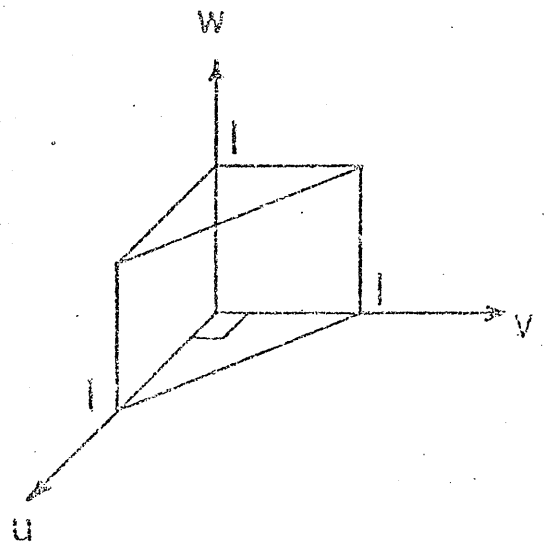

Fig. 4.4 The prism element

The volume integral

$$I_2 = \int_V f(x,y,z)\ dv = \int_{z_a}^{z_b} \int_{S_{xy}} f(x,y,z)\ dxdydz \qquad (4.40)$$

is to be evaluated. Analogous to the planar triangular surface finite elements, the surface S_{xy} is represented by the parametric expression

$$\begin{aligned} x &= \sum_{i=1}^{n} \alpha_i(u,v)\ x_i \\ y &= \sum_{i=1}^{n} \alpha_i(u,v)\ y_i \end{aligned} \qquad (4.41)$$

The surface integral over S_{xy} is therefore performed over the simplex in the u-v plane. The integral (4.40) is thus

$$I_2 = \int_0^1 \int_0^{1-v} \int_0^1 f(u,v,w)\ J_1 J_2\ du dv dw \tag{4.42}$$

where J_1 is the Jacobian

$$J_1 = \begin{vmatrix} \frac{\partial x}{\partial u} & \frac{\partial y}{\partial u} \\ \frac{\partial x}{\partial v} & \frac{\partial y}{\partial v} \end{vmatrix} \tag{4.43}$$

and $$J_2 = z_b - z_a. \tag{4.44}$$

As an example, the magnetic field due to a current density of 1 A/m^2 in a square conductor of Fig. 4.5 is calculated using the

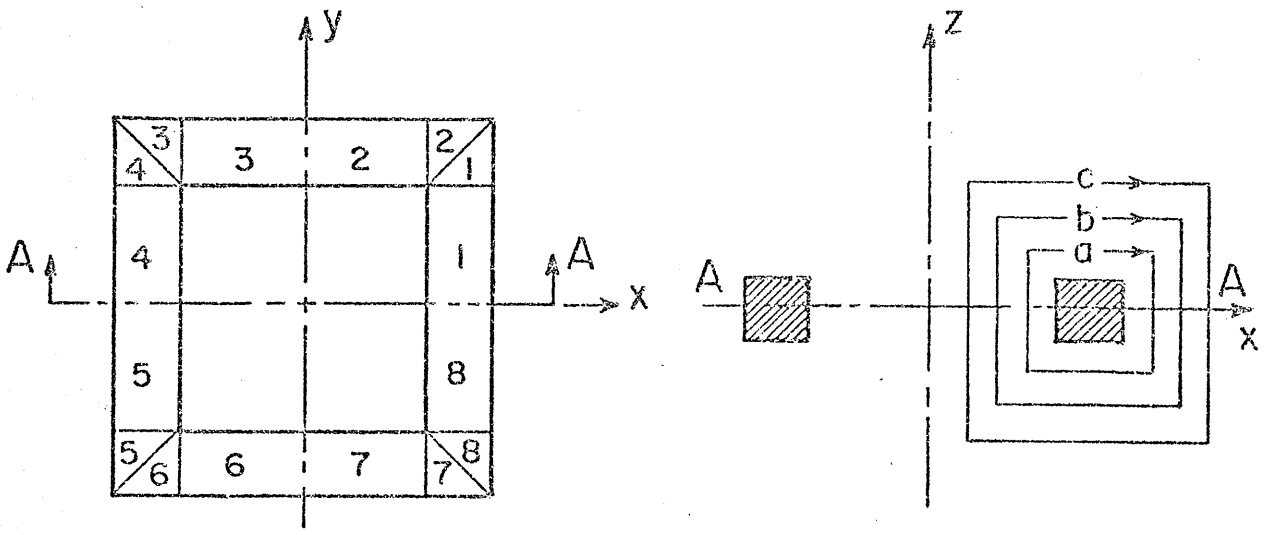

(a) (b) Cross-section at AA

Fig. 4.5 Element configuration of a square conductor

integration scheme described. The conductor is divided into 8 cube and 8 prism elements. The field at a point $\bar{r}$ is obtained by summing the contributions due to each and every element. Fig. 4.6 shows the computed field at y = 0. The accuracy of the computation is examined from the relationship

$$I = \oint \bar{H} \cdot \overline{d\ell} \tag{4.45}$$

Table 4.1 summarizes values of the contour integral (4.45) evaluated along the paths a, b and c shown in Fig. 4.5 using Simpson's $\frac{1}{3}$ rule. The agreement is satisfactory. However, it is appropriate to point out that experience in computing the source field for the magnet problem of Section 4.5 indicates that at points close to the conductor higher order Gaussian quadrature formula is needed.

TABLE 4.1

Values of contour integral (4.45)

	I(computed)	I(theorectical)
Path a	1.02475	1.00000
Path b	1.00226	1.00000
Path c	0.99930	1.00000

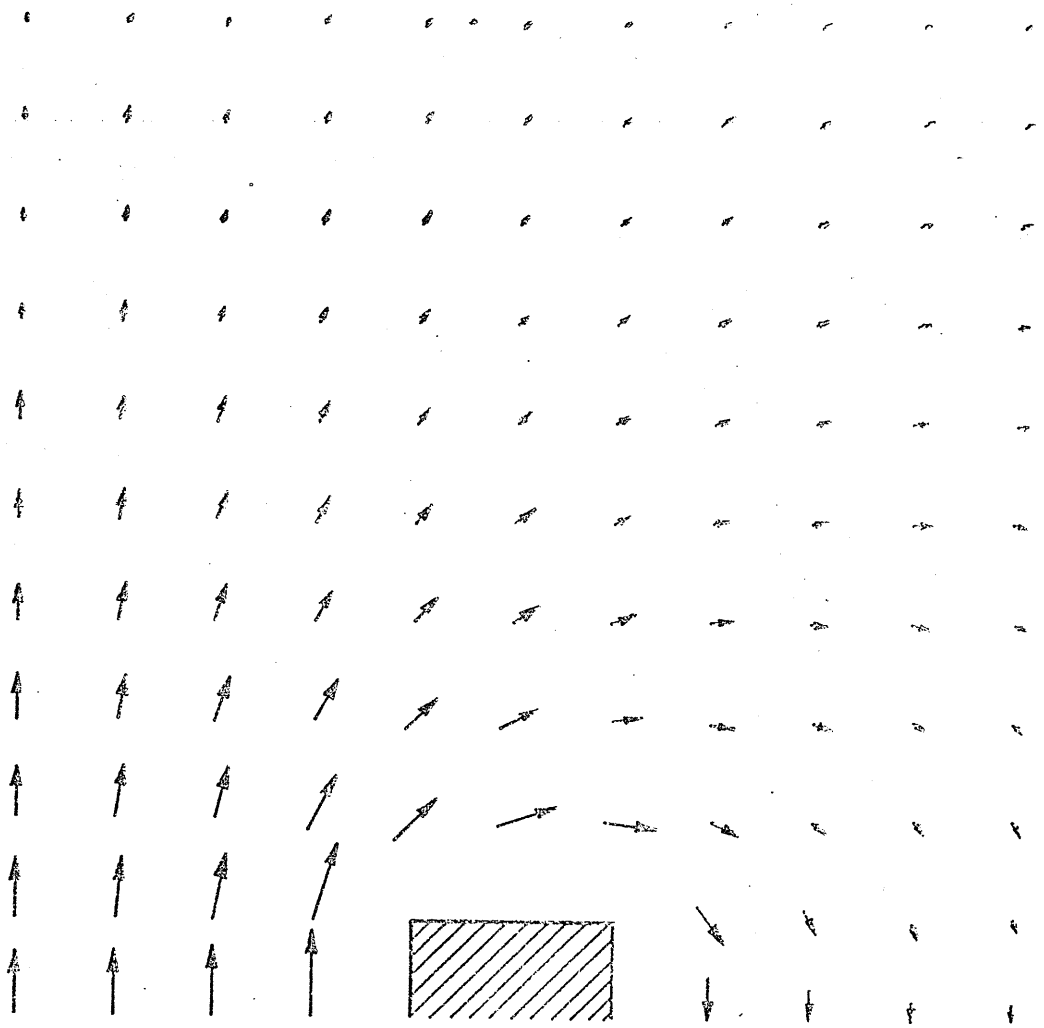

Fig. 4.6 H_c field at y = 0 of Fig. 4.5

4.4 PERMEABLE PROLATE SPHEROID IN UNIFORM FIELD

We will now illustrate the finite-element boundary integral approach by considering the problem of finding the field distribution resulting from a magnetic body immersed in a uniform impressed field. In this case, since the source field H_c has no circulation, it may be expressed as the gradient of a scalar function

$$\bar{H}_c = - \nabla\Psi \tag{4.46}$$

From (4.4) and (4.8), the resultant field in the presence of a permeable body may therefore be expressed in terms of a scalar potential as

$$\bar{H} = - \nabla\tilde{\phi} \tag{4.47}$$

where

$$\tilde{\phi} = \psi + \phi \tag{4.48}$$

Thus, in the special case of a uniform impressed field, the integral equation (4.26) may be written in terms of $\tilde{\phi}$.

Since ψ is harmonic inside the body, from Green's theorem, we have

$$\int_S G(s|s') \frac{\partial\psi}{\partial n}(s')\, ds' = \frac{\psi(s)}{2} + \int_S \psi(s') \frac{\partial G}{\partial n}(s|s')\, ds' \tag{4.49}$$

From (4.48) and (4.49), (4.26) therefore yields

$$-\frac{\mu_r+1}{2}\tilde{\phi}(s) + (\mu_r-1)\int_S \tilde{\phi}(s) \frac{\partial G}{\partial n}(s|s')\, ds' = \psi(s) \tag{4.50}$$

the solution of which gives directly the resultant field (in terms of $\tilde{\phi}$) due to the introduction of a permeable body in a uniform impressed field.

Once $\tilde{\phi}$ is known, from (4.28) and (4.30), the exterior and interior values of $\tilde{\phi}$ are computed by

$$\tilde{\phi}(\bar{r}) = \psi(\bar{r}) - (\mu_r - 1) \int_S \tilde{\phi}(s) \frac{\partial G}{\partial n} ds \tag{4.51}$$

and

$$\tilde{\phi}(\bar{r}) = \frac{\psi(\bar{r})}{\mu_r} - \frac{(\mu_r - 1)}{\mu_r} \int_S \tilde{\phi}(s) \frac{\partial G}{\partial n} ds \tag{4.52}$$

respectively.

Fig. 4.7 depicts the problem of a prolate spheroid of principal semi-axis a = b = 1, c = 2 and of relative permeability μ_r placed in a uniform field of unit intensity parallel to the x-y plane.

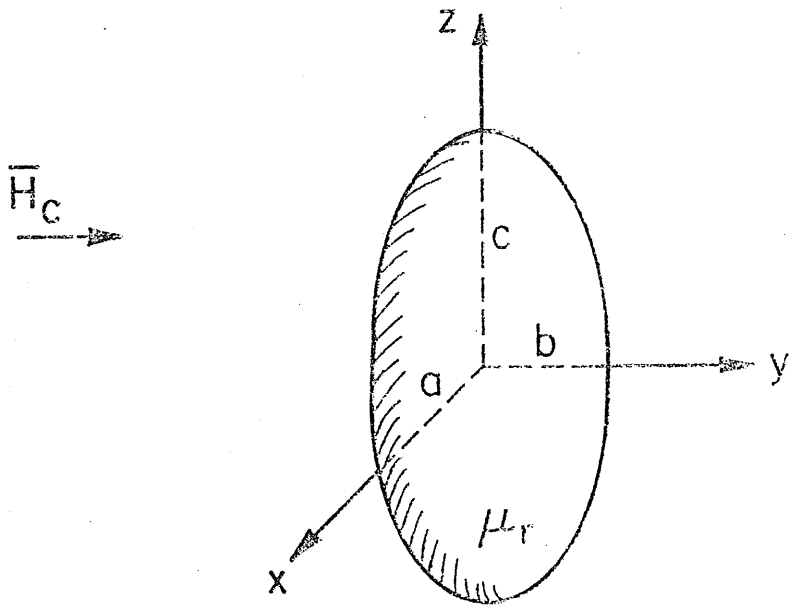

Fig. 4.7 A permeable prolate spheroid in uniform field

With symmetry about the z = 0 plane and antisymmetry about the y = 0 plane, the problem is solved in the positive quadrant only, i.e., over one-eighth of the surface. The positive quadrant surface is divided into triangular elements. Fig. 4.8 shows the finite-element model having 14 elements.

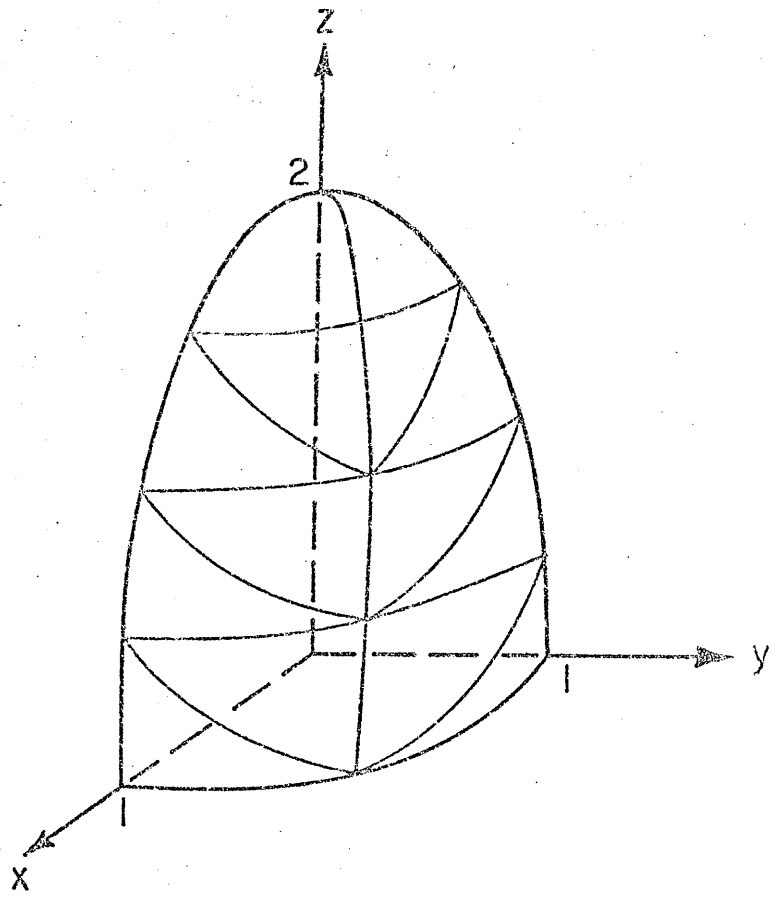

Fig. 4.8 A finite-element model of the problem of Fig. 4.7

To generate the matrix system for (4.50), the algorithm described in detail in Chapter II is applied. From (2.31), the matrix equation for the kth element is

$$\frac{\mu_r+1}{2}\int_{S_k}\underline{\alpha}(s)\underline{\alpha}^T(s)\,ds\,\tilde{\underline{\phi}}_k + (\mu_r-1)\int_{S_k}\underline{\alpha}(s)\sum_{j=1}^{t}\int_{S_j}\underline{\alpha}^T(s)\,\frac{\partial G}{\partial n}(s|s')\,ds'ds\,\tilde{\underline{\phi}}_j$$

$$= \int_{S_k}\underline{\alpha}(s)\,\psi(s)\,ds \qquad (4.53)$$

where t is the total number of elements. The system of equations (4.53) is generated for each element in turn and is accumulated to produce the global system for the complete structure. The singular integral in this case corresponding to the kernel $\frac{\partial G}{\partial n}(s|s')$ has the form

$$I = \int_R \frac{(x-x_p)}{|\bar{r}-\bar{r}_p|^3}\,ds \qquad (4.54)$$

which is evaluated in the t-u-v coordinate system of Fig. 2.6 as

$$I = \int_{t_b}^{t_a}\int_{f_a(t)}^{f_c(t)} \frac{(\beta t+\gamma u)}{(\sqrt{t^2+u^2})^3}dudt + \int_{t_a}^{t_c}\int_{f_a(t)}^{f_b(t)} \frac{(\beta t+\gamma u)}{(\sqrt{t^2+u^2})^3}dudt \qquad (4.55)$$

where β and γ are the components of the vector $(x-x_p)$ in the t and u directions, respectively. Let $f(t) = mt + n$. The integral

$$I = \int_{T_1}^{T_2}\int_{m_1t+c_1}^{m_2t+c_2} \frac{(\beta t+\gamma u)}{(\sqrt{t^2+u^2})^3}dudt \qquad (4.56)$$

has the closed-form expression given by

$$I = \frac{\beta m_2 - \gamma}{\sqrt{m_2^2 + 1}} \sinh^{-1} \frac{(m_2^2+1)T_2 + c_2 m_2}{|c_2|} + \frac{-\beta m_1 + \gamma}{\sqrt{m_1^2 + 1}} \sinh^{-1} \frac{(m_1^2+1)T_2 + c_1 m_1}{|c_1|}$$

$$+ \beta \log \left[\frac{2c_2}{T_1} \left(\sqrt{(m_2^2+1)T_1^2 + 2c_2 m_2 T_1 + c_2^2} + m_2 T_1 + c_2\right)\right]$$

$$- \beta \log \left[\frac{2c_2}{T_2} \left(\sqrt{(m_2^2+1)T_2^2 + 2c_2 m_2 T_2 + c_2^2} + m_2 T_2 + c_2\right)\right]$$

$$- \beta \log \left[\frac{2c_1}{T_1} \left(\sqrt{(m_1^2+1)T_1^2 + 2c_1 m_1 T_1 + c_1^2} + m_1 T_1 + c_1\right)\right]$$

$$+ \beta \log \left[\frac{2c_1}{T_2} \left(\sqrt{(m_1^2+1)T_2^2 + 2c_1 m_1 T_2 + c_1^2} + m_1 T_2 + c_1\right)\right]$$

$$+ \frac{-\beta m_2 + \gamma}{\sqrt{m_2^2+1}} \sinh^{-1} \frac{(m_2^2+1)T_1 + c_2 m_2}{|c_2|} + \frac{\beta m_1 - \gamma}{\sqrt{m_1^2 + 1}} \sinh^{-1} \frac{(m_1^2+1)T_1 + c_1 m_1}{|c_1|} \qquad (4.57)$$

The integral of (4.55) are computed directly from (4.57).

Fig. 4.9 shows contours of constant $\tilde{\phi}$ at x = 0 in the presence of the prolate spheroidal body with relative permeability $\mu_r = 10$ using second-order approximation with 39 nodes. As expected, a uniform field of reduced intensity is observed inside the magnetic body.

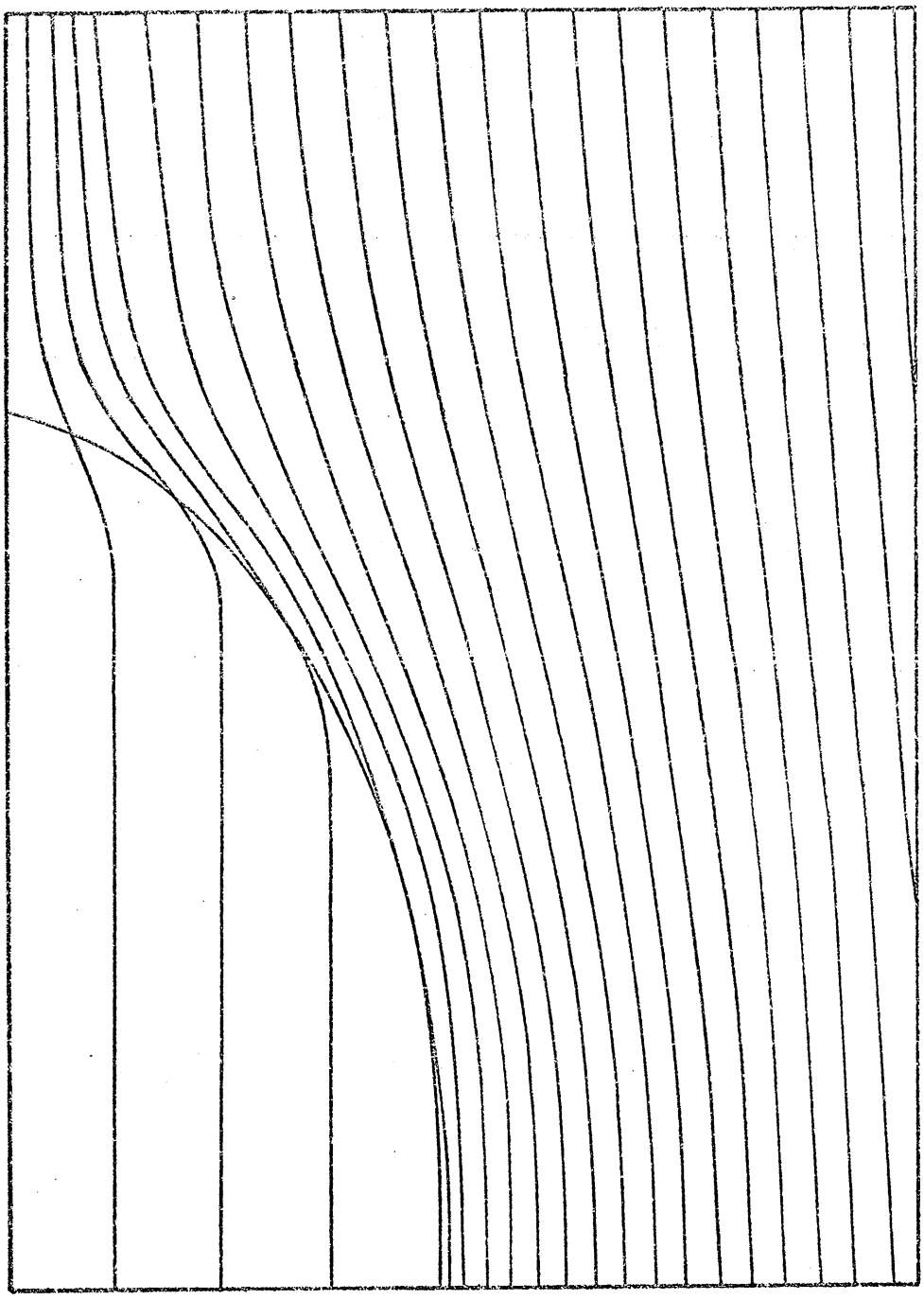

Fig. 4.9 Equipotential contour at x = 0

To show the instability of the exterior ϕ expression, the problem is also solved using equation (4.26) for the scalar potential due to polarization. From the boundary solution, the values of ϕ in the regions interior and exterior to the magnetic material are then computed from (4.28) and (4.30). Tables 4.2 and 4.3 summarize the computed values of ϕ at a set of observation points (x,y,z).

It is obvious from the values of Table 4.2 that for the high permeability case of $\mu = 1000$, a small deviation in the solution could lead to a large change in the computed values of ϕ. For example, the field at an observation point $x = z = 0$, $y = 1.1$ is to be computed. Using the solution of (4.26), equation (4.30), that is

$$\phi(\bar{r}) = (\mu_r - 1) \left[\int_S G(\bar{r}|s)\, H_{cn}(s)\, ds - \int_S \phi(s)\, \frac{\partial G}{\partial n}(\bar{r}|s)\, ds\right] \qquad (4.60)$$

has the numeric values

$$\phi(\bar{r}) = 999 \times (.320085 - .319562)$$

$$= .522477 \qquad (4.61)$$

The boundary solution of (4.26) appears in the second integral of the right-hand side of (4.60). Note that with 1% deviation in the second integral of (4.60), the computed value of (4.60) is

$$\phi(\bar{r}) = 999 \times (.320085 - .316366)$$

$$= 3.71493 \qquad (4.62)$$

TABLE 4.2

Analysis of exterior ϕ values at (0,y,0) (μ=1000)

$A = \int GH_{cn}\, ds$

$B = \int \phi \frac{\partial G}{\partial n}\, ds$

$\phi = (\mu-1)(A-B)$

$\phi_d = (\mu-1)(A-.99B)$

Deviation (%) = $100(|\phi_d-\phi|)/\phi$

y	A	B	A-B	ϕ	ϕ_d	Deviation (%)
1.1	.320085	.319562	5.23001×10^{-4}	.522477	3.71493	611.0
1.2	.278831	.278317	5.14001×10^{-4}	.513487	3.29388	541.5
1.3	.245938	.245456	4.81993×10^{-4}	.481511	2.93364	509.3
1.4	.218746	.218301	4.44993×10^{-4}	.444548	2.62539	490.6
1.5	.195849	.195440	4.08992×10^{-4}	.408583	2.36104	477.9
1.6	.176332	.175957	3.75003×10^{-4}	.374628	2.13244	469.2
1.7	.159542	.159199	3.43010×10^{-4}	.342667	1.93307	464.1
1.8	.144990	.144674	3.16009×10^{-4}	.315693	1.76100	457.8
1.9	.132294	.132003	2.90990×10^{-4}	.290699	1.60941	453.6
2.0	.121154	.120886	2.67997×10^{-4}	.267729	1.47538	451.1

TABLE 4.3

Analysis of exterior ϕ values at (0,y,0) (μ=10)

$A = \int GH_{cn}\, ds$

$b = \int \phi \frac{\partial G}{\partial n}\, ds$

$\phi = (\mu-1)(A-B)$

$\phi_d = (\mu-1)(A-.99B)$

Deviation (%) = $100(|\phi_d-\phi|)/\phi$

y	A	B	A-B	ϕ	ϕ_d	Deviation (%)
1.1	.320085	.251910	.068175	.613575	.636247	3.69
1.2	.278831	.219510	.059321	.533889	.553645	3.70
1.3	.245938	.193639	.052299	.470691	.488119	3.70
1.4	.218746	.172236	.04651	.418590	.434091	3.70
1.5	.195849	.154217	.041632	.374688	.388568	3.70
1.6	.176332	.138836	.037496	.337464	.349959	3.70
1.7	.159542	.125612	.033930	.305370	.316675	3.70
1.8	.144990	.114150	.030840	.277560	.287834	3.70
1.9	.132294	.104150	.028144	.253296	.262669	3.70
2.0	.121154	.0953765	.025777	.231998	.240581	3.70

The change in ϕ from (4.61) to (4.62) amounts to 611%. The ill-conditioned behaviour of the system is thus evident from (4.61) and (4.62). Because of the factor (μ-1) in (4.60), the extent of ill-conditioning increases with increased permeability. For the particular example of uniform impressed field considered, the scalar potential ψ is known, the total field $\tilde{\phi}$ is therefore readily obtainable from the expression

$$\tilde{\phi} = \phi + \psi \tag{4.63}$$

With (4.51), the exterior ϕ values can also be computed by

$$\phi(\bar{r}) = -(\mu_r - 1) \int_S \tilde{\phi}(s) \frac{\partial G}{\partial n} \, ds \tag{4.64}$$

It then appears that (4.64) would be a more stable method for computing exterior fields. However, unfortunately this is not always true. Expression (4.64) yields a satisfactory result only if $\tilde{\phi}$ is obtained directly as the solution of the integral equation (4.50) (because, in this case, the error in computing the ϕ values is compatible to the error of the solution $\tilde{\phi}$). On the other hand, for $\tilde{\phi}$ obtained from the solution ϕ by (4.63), the error in computing ϕ using (4.64) will be magnified implicitly as seen below.

Applying Green's theorem, we have

$$\int_S [G(\bar{r}|s) \frac{\partial \psi}{\partial n} - \psi(s) \frac{\partial G}{\partial n} (\bar{r}|s)] \, ds = 0$$

Equation (4.64) can therefore be expressed as

$$\phi(\bar{r}) = (\mu_r - 1) \left[-\int_S G(\bar{r}|s) \frac{\partial \psi}{\partial n} \, ds - \int_S \phi(s) \frac{\partial G}{\partial n} (\bar{r}|s) \, ds \right] \qquad (4.65)$$

which is mathematically as well as numerically identical to (4.60). The ill-conditioned behaviour therefore remains with (4.64).

However, the unstable behaviour does not occur in computing interior ϕ values as is evident from Tables 4.4 and 4.5. The interior expression is numerically stable and results obtained are satisfactory.

In the following, an alternate expression in place of (4.60) is derived.

From (4.60), we have

$$\frac{\phi}{\mu - 1} = \int_S G \, H_{cn} \, ds - \int_S \phi \frac{\partial G}{\partial n} \, ds \qquad (4.66)$$

Since ϕ is harmonic, consider an observation point exterior to the permeable body, we have

$$\phi = -\int_S G \frac{\partial \phi}{\partial n} \, ds + \int_S \phi \frac{\partial G}{\partial n} \, ds \qquad (4.67)$$

where n is the outward normal to the body as previously defined. Combining (4.66) and (4.67) yields

$$\phi = \frac{\mu - 1}{\mu} \left[\int_S G \, H_{cn} \, ds - \int_S G \frac{\partial \phi}{\partial n} \, ds \right] \qquad (4.68)$$

TABLE 4.4

Analysis of interior ϕ values at (0,y,0) (μ=1000)

$A = \int GH_{cn}\, ds$

$B = \int \phi \frac{\partial G}{\partial n}\, ds$

$\phi = (\mu-1)(A-B)/\mu$

$\phi_d = (\mu-1)(A-.99B)/\mu$

Deviation (%) = $100(|\phi_d-\phi|)/\phi$

y	A	B	A-B	ϕ	ϕ_d	Deviation (%)
0.1	.041512	-.058373	.099885	.0997851	.099202	.584
0.2	.083029	-.116742	.199771	.199571	.198405	.584
0.3	.124551	-.175108	.299659	.299359	.297610	.584
0.4	.166060	-.233490	.39955	.399150	.396818	.584
0.5	.207477	-.291968	.499445	.498946	.496029	.585
0.6	.248593	-.350758	.599351	.598752	.595248	.585
0.7	.288931	-.410344	.699275	.698576	.694476	.587
0.8	.327478	-.471753	.799231	.798432	.793719	.590
0.9	,361891	-.537260	.899151	.898252	.892884	.597

TABLE 4.5

Analysis of interior ϕ values at (0,y,0) (μ=10)

$A = \int GH_{cn}\, ds$

$B = \int \phi \frac{\partial G}{\partial n}\, ds$

$\phi = (\mu-1)(A-B)/\mu$

$\phi_d = (\mu-1)(A-.99B)/\mu$

Deviation (%) = $100(|\phi_d-\phi|)/\phi$

y	A	B	A-B	ϕ	ϕ_d	Deviation (%)
0.1	.0415120	-.0460583	.087570	.078813	.078399	.526
0.2	.0830289	-.0921119	.175141	.157627	.156798	.526
0.3	.124551	-.138160	.262711	.23644	.235196	.526
0.4	.166060	-.184216	.350276	.315248	.313590	.526
0.5	.207477	-.230340	.437817	.394035	.391962	.526
0.6	.248593	-.276693	.525286	.472757	.470267	.527
0.7	.288931	-.323637	.612568	.551311	.548398	.528
0.8	.327478	-.371938	.699416	.629474	.626127	.532
0.9	.361891	-.423309	.785200	.706680	.702870	.539

The factor $(\mu-1)/\mu$ in (4.68) tends to unity with increasing permeability whereas in (4.60), the factor $(\mu-1)$ increases with μ. Therefore, the difficulty associated with the subtraction of two almost identical numbers does not arise with (4.68) as is the case with (4.60) for large μ. Thus equation (4.68) is a more stable formulation than that given by (4.60). However, (4.68) involves the $\frac{\partial\phi}{\partial n}$ term. This suggests that a two-field formulation solving both ϕ and $\frac{\partial\phi}{\partial n}$ directly would be preferable, i.e., equation (4.15) is applied to solve for both ϕ and $\frac{\partial\phi}{\partial n}$. In the following section, a magnet problem is solved in which the airgap field is derived from the $\frac{\partial\phi}{\partial n}$ solution. The numerical data obtained further justifies the above analysis.

4.5 A MAGNET

The integral finite-element method will now be applied to a more complicated structure. Fig. 4.10 shows a c-shaped magnet with circular cross-section tapered poles. Two cylindrical conductors each carrying a current of density 3 A/m^2 are placed coaxial with the top and bottom poles. For this problem, the solution procedures consist of two parts. First, the free space source field H_c (that is, the field in the absence of the magnet) is to be computed. Equation (4.26) with the right-hand side containing the known source term is then solved for the magnetic potential due to polarization. In this case, since $\nabla \times H_c \neq 0$, the resultant field can not be represented by the scalar function $\tilde{\phi}$ as for the case of the uniform impressed field of Section 4.4.

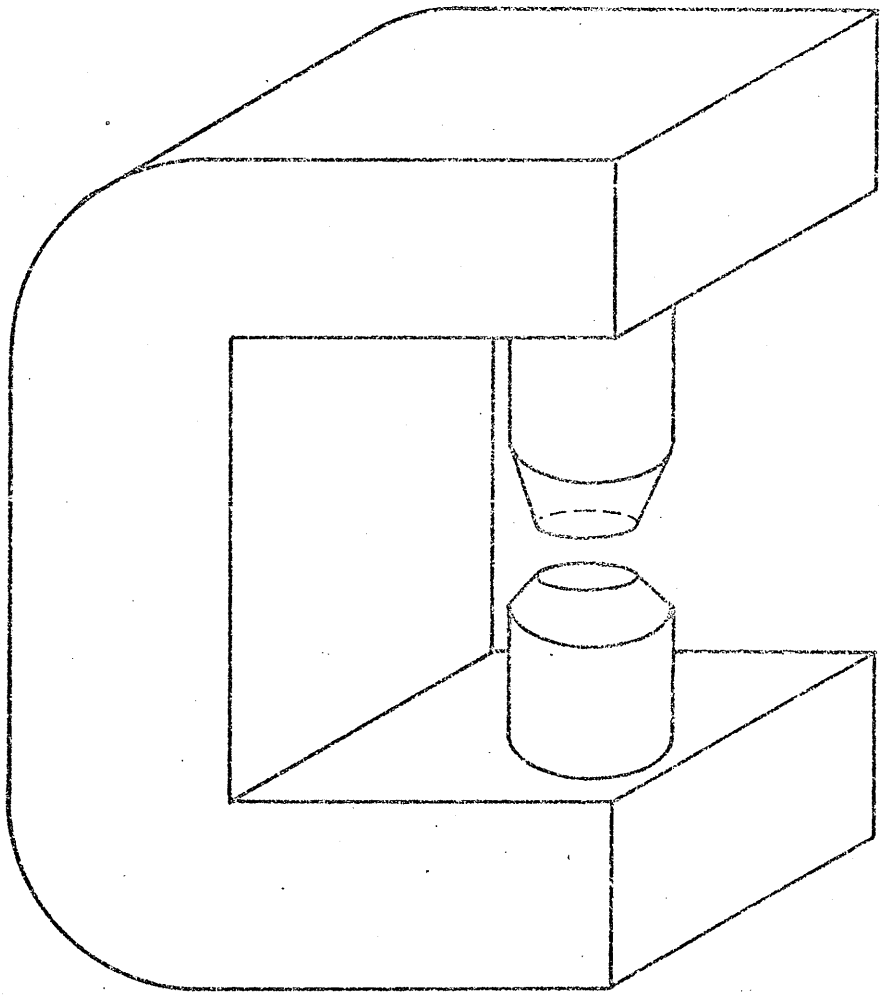

Fig. 4.10 A magnet

To compute $\bar{H}_c$, the prism element described in Section 4.3 is used. By symmetry, only one-quarter of the problem is considered. Fig. 4.11 shows the cross-sectional view of the element arrangement in one quarter

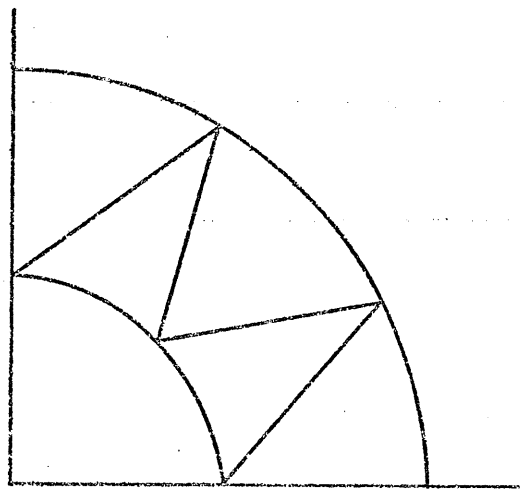

Fig. 4.11 Cross-sectional view of the prism elements for the coil.

of the coil. Fig. 4.12 shows the finite-element model used for the magnet of Fig. 4.10. The algorithm for evaluating the volume integral

$$\bar{H}_c = \frac{1}{4\pi} \int \frac{J \times (\bar{r}-\bar{r}')}{|\bar{r}-\bar{r}'|^3} \, dv \qquad (4.58)$$

is described in Section 4.3. From (4.26), values of $\bar{H}_c$ are to be obtained at the Gaussian points of each magnet element. Gaussian quadrature of order 11 was used in the evaluation of (4.58). For points at a greater distance away from the coil, lower-order quadrature formula has been proved satisfactory. However, higher-order formula is generally needed

in computing values of $\bar{H}_c$ at points underneath the coil. Fig. 4.13 shows the convergence of the integrated value with increased quadrature order at an arbitrary Gaussian point (33., -36.3, 92.4).

For the finite-element model shown in Fig. 4.12, there are 73 elements and 49 vertex nodes. From (2.31), the matrix equation, corresponding to the integral equation (4.26), for a single element, say, the kth element is

$$\frac{\mu_r+1}{2}\int_{S_k}\underline{\alpha}(s)\underline{\alpha}^T(s)\,ds\;\underline{\phi}_k + (\mu_r-1)\int_{S_k}\underline{\alpha}(s)\sum_{j=1}^{t}\int_{S_j}\underline{\alpha}^T(s')\frac{\partial G}{\partial n}(s|s')\,ds'ds\;\underline{\phi}_j$$

$$= (\mu_r-1)\int_{S_k}\underline{\alpha}(s)\int_{S}G(s|s')\,H_{cn}(s')\,ds'ds \qquad (4.59)$$

Equations (4.59) are generated for each element in turn as in all previous analysis. They are then assembled to yield the global system. Fig. 4.14 shows a sketch of the contours of ϕ in the interior region. To obtain the field in the airgap, the two-field formulation (4.15) involving ϕ and $\frac{\partial\phi}{\partial n}$ is applied. Values of ϕ having same order of accuracy as that derived from the single-field expression is obtained. Figure 4.15 shows a plot of the z-component of the magnetic field intensity in a plane in the airgap midway between the poles.

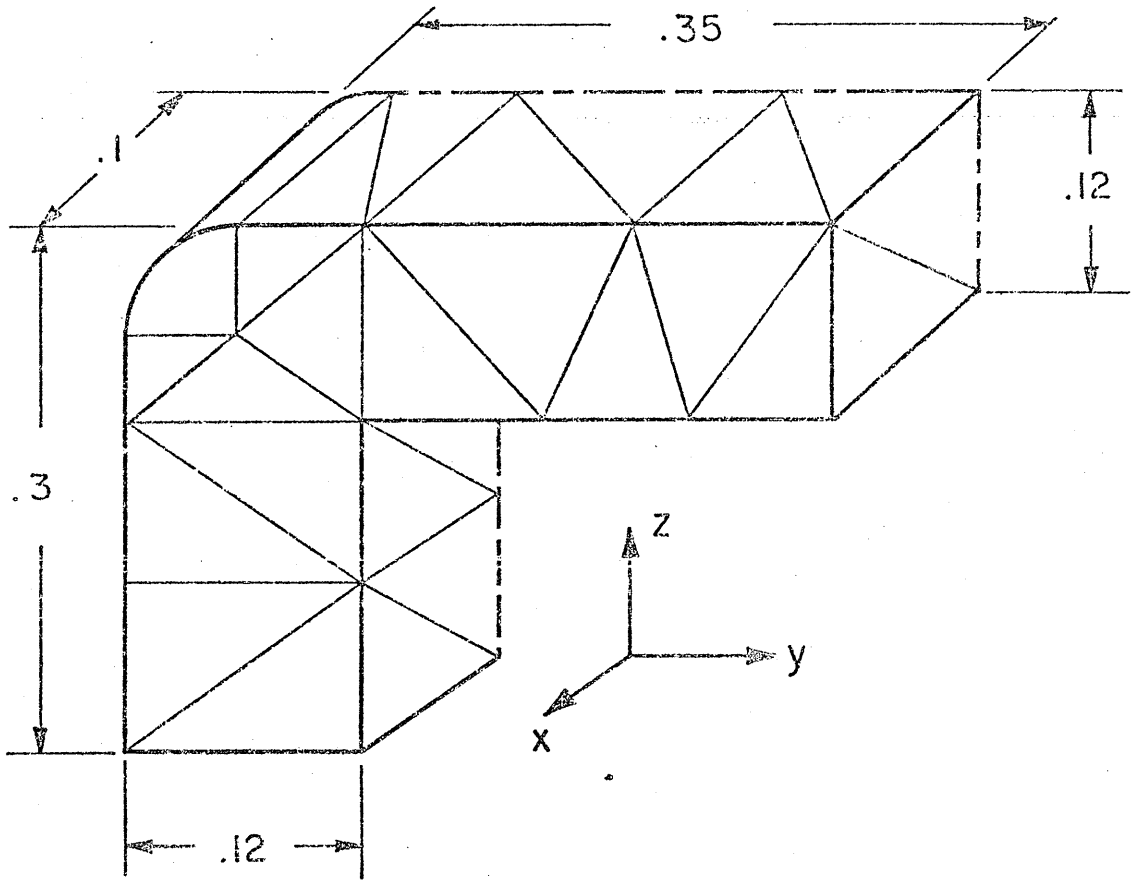

Fig. 4.12 Finite-element model of the magnet

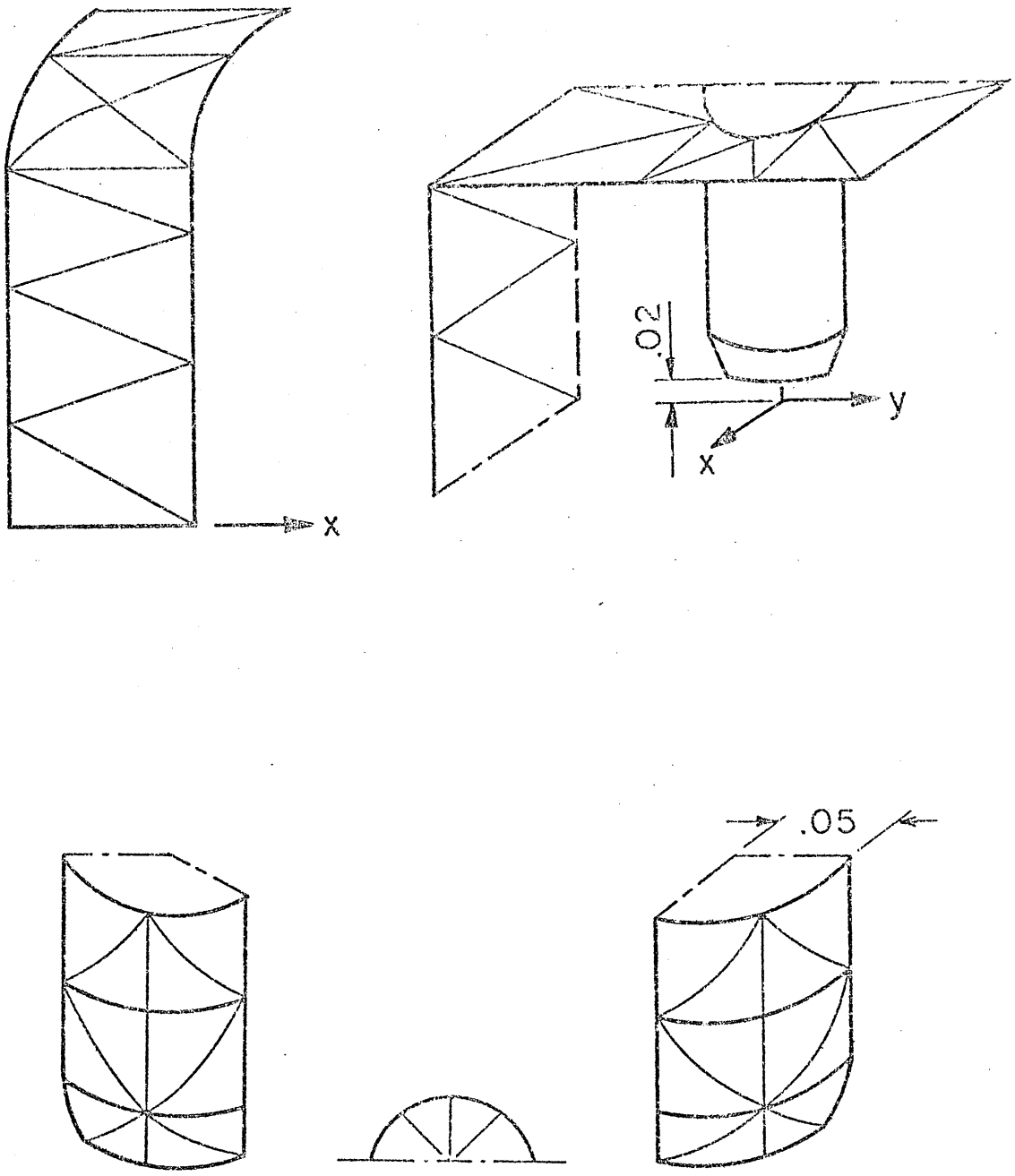

Fig. 4.12 (continued)

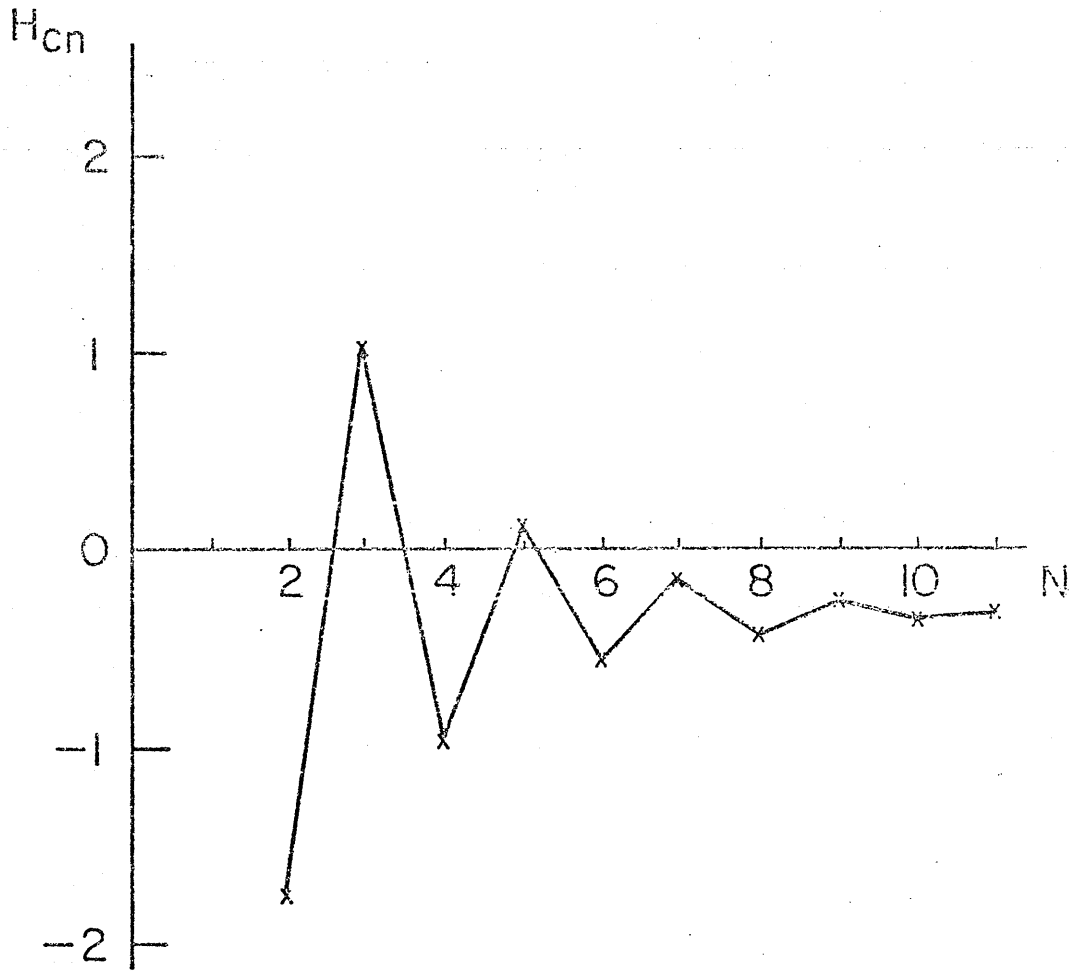

Fig. 4.13 Characteristic of H_{cn} as a function of quadrature order at a point on the magnet pole face.

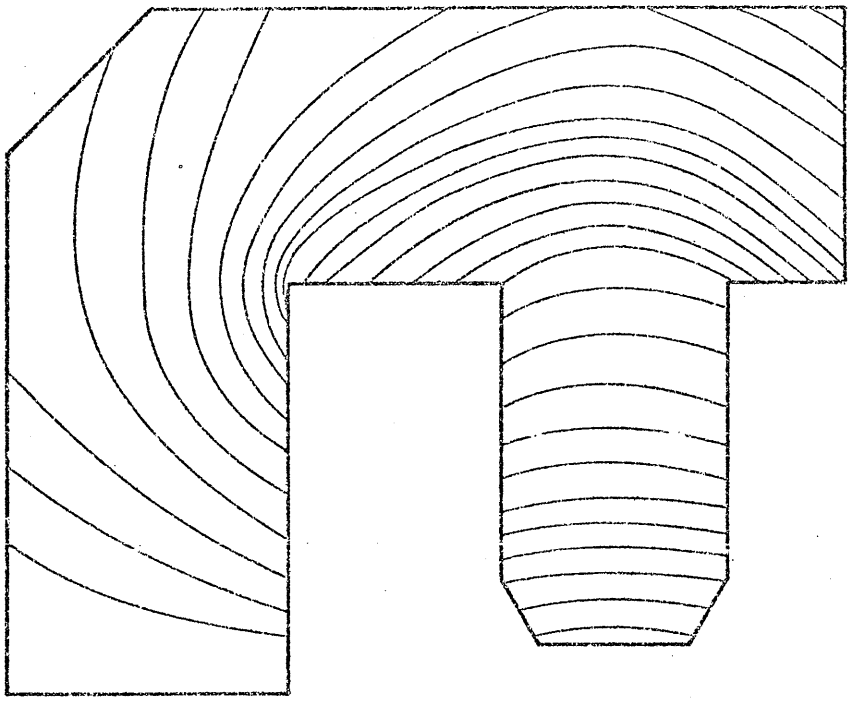

Fig. 4.14 Contours of Constant ϕ at x = 0

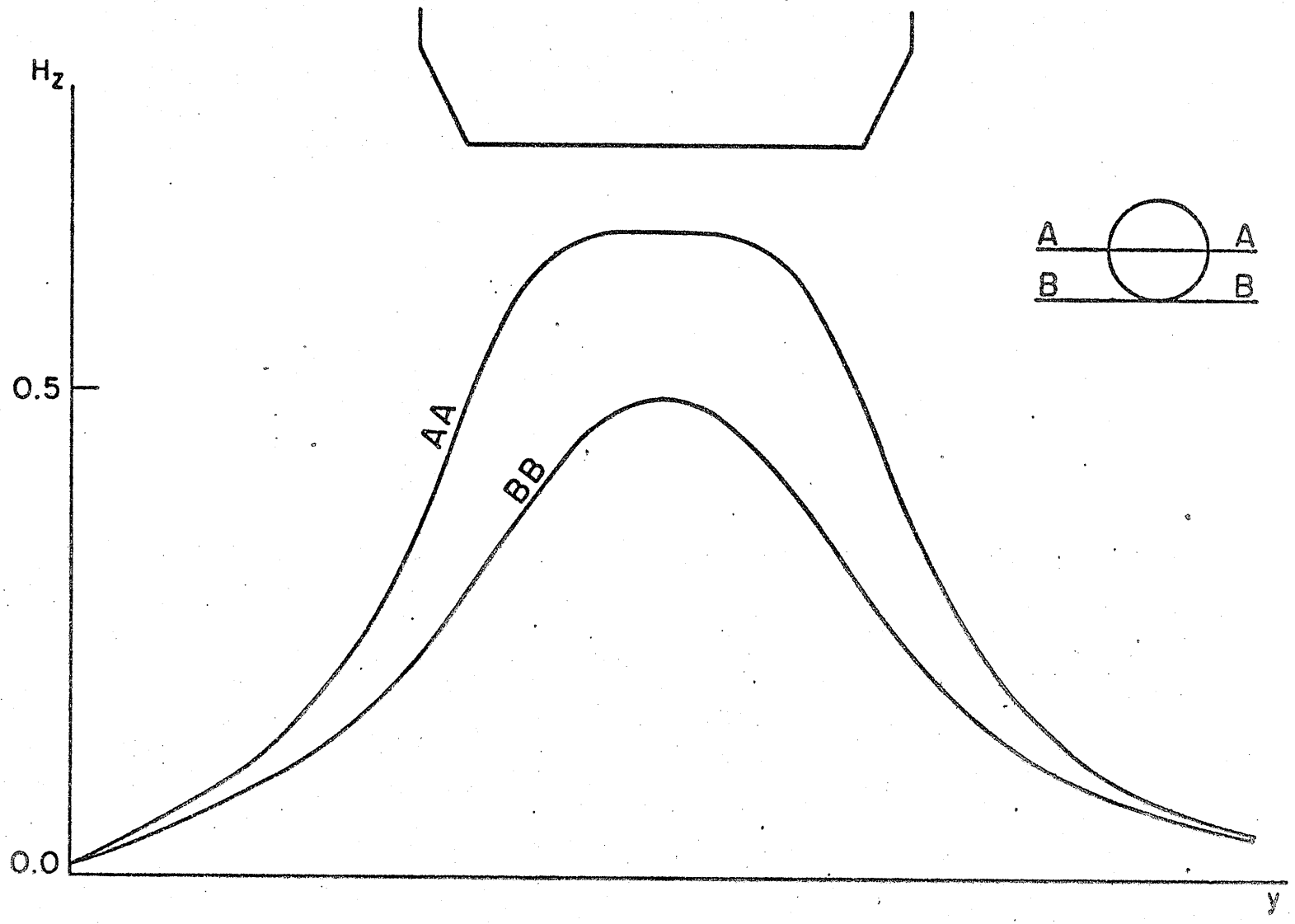

Fig. 4.15 Magnetic field intensity in the airgap along z=0

CHAPTER V

DISPLACEMENT PROBLEMS IN THREE-DIMENSIONAL ELASTOSTATICS — A VECTOR FIELD

The method developed in Chapter II is by no means limited to the solution of scalar fields. Extension to vector fields is fairly direct. To illustrate the application of the technique to vector fields, the displacement problem in three-dimensional elastostatics is considered. For three-dimensional vector formulations, three degrees of freedom are associated with each finite-element node resulting in three times the number of equations of that required in the scalar case.

5.1 BASIC FIELD EQUATIONS

The partial differential equation which governs the elastostatic field distribution within an elastic body R is given by

$$\mu\nabla^2\bar{u} + (\lambda+\mu)\nabla\nabla\cdot\bar{u} + \rho\bar{b} = 0 \tag{5.1}$$

where $\bar{u} = [u_1, u_2, u_3]^T$ is the displacement vector with u_1, u_2 and u_3 being the x_1, x_2 and x_3 components, respectively. λ, μ are Lame's constants, ρ is the mass density and $\bar{b} = [b_1, b_2, b_3]^T$ are the body forces in the three directions. For three-dimensional problems, (5.1) is formed from three equations which can be expressed more explicitly as

$$\mu\nabla^2 u_1 + (\lambda+\mu)\frac{\partial}{\partial x_1}\left(\frac{\partial u_1}{\partial x_1} + \frac{\partial u_2}{\partial x_2} + \frac{\partial u_3}{\partial x_3}\right) + \rho b_1 = 0$$

$$\mu\nabla^2 u_2 + (\lambda+\mu)\frac{\partial}{\partial x_2}\left(\frac{\partial u_1}{\partial x_1} + \frac{\partial u_2}{\partial x_2} + \frac{\partial u_3}{\partial x_3}\right) + \rho b_2 = 0 \qquad (5.2)$$

$$\mu\nabla^2 u_3 + (\lambda+\mu)\frac{\partial}{\partial x_3}\left(\frac{\partial u_1}{\partial x_1} + \frac{\partial u_2}{\partial x_2} + \frac{\partial u_3}{\partial x_3}\right) + \rho b_3 = 0$$

Here, the Dirichlet boundary-value problem will be considered where the displacement components are prescribed on the boundary. The complete problem is therefore posed in the partial differential formulation as

$$\begin{aligned} &\mu\nabla^2\bar{u}(\bar{r}) + (\lambda+\mu)\nabla\nabla\cdot\bar{u}(\bar{r}) + \rho\bar{b}(\bar{r}) = 0 \qquad \bar{r} \in R \\ &\bar{u}(s) = \bar{g}(s) \qquad s \in S \end{aligned} \qquad (5.3)$$

where S is the boundary of R. When there are no body forces, we have

$$\begin{aligned} &\mu\nabla^2\bar{u}(\bar{r}) + (\lambda+\mu)\nabla\nabla\cdot\bar{u}(\bar{r}) = 0 \qquad \bar{r} \in R \\ &\bar{u}(s) = \bar{g}(s) \qquad s \in S \end{aligned} \qquad (5.4)$$

5.2 BOUNDARY INTEGRAL EQUATION FORMULATION

The Green's function to the operator of (5.1), i.e., the solution to (5.1) with the source being a unit force applied in each direction at a point, say $\bar{r}'$, is [44]

$$\bar{\bar{G}}(\bar{r}|\bar{r}') = \frac{1}{8\pi\mu(\lambda+2\mu)}\left(\frac{\lambda+3\mu}{|\bar{r}-\bar{r}'|}\bar{\bar{I}} + \frac{\lambda+\mu}{|\bar{r}-\bar{r}'|^3}\bar{\bar{R}}\right) \qquad (5.5)$$

where $\bar{\bar{I}} = \hat{u}_i \hat{u}_i$

and $\bar{\bar{R}} = (x_i - x_i')(x_j - x_j')\hat{u}_i \hat{u}_j$

with summation i,j = 1,2,3 over the coordinates understood, $\hat{u}_i$ and $\hat{u}_j$ are unit vectors. From the definition of the Green's function, the displacements due to a source density $\bar{b}(\bar{r})$ are therefore given by

$$\bar{u}(\bar{r}) = \int_R \bar{\bar{G}}(\bar{r}|\bar{r}') \cdot \bar{b}(\bar{r}') \, d\Omega \tag{5.6}$$

where the integration is performed over the entire region where sources are present.

Analogous to the theory of electrostatic potential, the Dirichlet problem (5.4) may be formulated in terms of an equivalent source distribution on the boundary. Instead of solving for the displacements directly, one finds the equivalent force distribution by imposing the constraint that the displacements produced by the force satisfy prescribed boundary values.

Denoting by $\bar{f}(s)$ the equivalent source on the boundary, from (5.6), the displacements due to this source are given by

$$\bar{u}(\bar{r}) = \int_R \bar{\bar{G}}(\bar{r}|\bar{s}) \cdot \bar{f}(s) \, ds \tag{5.7}$$

Since, on the boundary, the condition $\bar{u}(s) = \bar{g}(s)$ is to hold, (5.7) is therefore

$$\int_R \bar{\bar{G}}(s|s') \cdot \bar{f}(s')\, ds' = \bar{g}(s) \tag{5.8}$$

Equation (5.8) is an integral equation in the unknown $\bar{f}$.

5.3 INTEGRAL FINITE-ELEMENTS FOR VECTOR FIELDS

The integral finite-element approach of previous chapters is described here for vector fields. The extension from the scalar to the vector case is fairly straightforward and obvious, although the procedure is more involved and complicated than for the scalar case.

The functional for the vector problem (5.8) is

$$F = \int_R \bar{f}(s) \cdot \int_R \bar{\bar{G}}(s|s') \cdot \bar{f}(s')\, ds' ds - 2 \int_R \bar{f}(s) \cdot \bar{g}(s)\, ds \tag{5.9}$$

Expression (5.9) is obtained by application of (2.7). Following the same line of approximation as for the scalar case, the unknown force function is expressed in terms of its values, yet unknown, associated with specified nodal points. To conveniently describe the procedure of discretization, consider, for the moment, all elements to be disjoint. Consider also that all nodes and interpolating polynomials of this disjoint structure are uniquely numbered, even including nodes that are to be coalesced when the structure is reassembled. Thus

$$\bar{f}(s) = \underline{\alpha}^T(s)\, \underline{\bar{f}} = \underline{\bar{f}}^T \underline{\alpha}(s) \tag{5.10}$$

where $\underline{\alpha}$ and $\underline{\bar{f}}$ are column vectors of order equal to M times the total number of elements with M related to the degree of polynomial approximation

N by

$$M = \frac{1}{2}(N+1)(N+2)$$

Moreover, for this vector case, each entry to $\underline{\bar{f}}$, say the kth entry $\bar{f}_k$, is a vector of the three components of $\bar{f}$ at the kth nodal point.

The $\underline{\bar{f}}$ terms are to take on values such that the functional (5.9) is rendered stationary. To accomplish this, substitute (5.10) into (5.9). Thus

$$F = \underline{\bar{f}}^T \cdot \int_R \underline{\alpha}(s) \int_R \underline{\underline{\bar{G}}}(s|s') \, \underline{\alpha}^T(s') \, ds' ds \cdot \underline{\bar{f}} - 2\underline{\bar{f}}^T \cdot \int_R \underline{\alpha}(s) \, \bar{g}(s) \, ds \tag{5.11}$$

The stationarity is obtained by differentiating the functional (5.11) with respect to each variational parameter in turn with each resulting equation set to zero. This is conveniently represented by

$$\frac{\partial F}{\partial \underline{\bar{f}}} = 0 \tag{5.12}$$

which results in

$$\int_R \underline{\alpha}(s) \int_R \underline{\underline{\bar{G}}}(s|s') \, \underline{\alpha}^T(s') \, ds' ds \cdot \underline{\bar{f}} = \int_R \underline{\alpha}(s) \, \bar{g}(s) \, ds \tag{5.13}$$

Separating the vector quantities into their individual components, (5.13) is a matrix equation of the form

$$S\underline{f} = \underline{b} \tag{5.14}$$

consisting of scalar entries but the order is three times that of the analogous scalar problem. In generating S and $\underline{b}$, matrix entries corresponding to individual nodes that coalesce, when the structure is reassembled, are accumulated into row and column numbers that correspond to the global numbering scheme. The construction of (5.14) is accomplished on an element-by-element basis.

The numerical integration scheme for generating the S and $\underline{b}$ matrices is described in Section 2.5. The singular integrals in this case, related to the dyadic Green's function (5.5), are

$$I_1 = \int_R \frac{1}{|\bar{r}-\bar{r}_p|}\, ds \tag{5.15}$$

and

$$I_2 = \int_R \frac{(x-x_p)^2}{|\bar{r}-\bar{r}_p|^3}\, ds \tag{5.16}$$

The expression for the integral (5.15) is given in (2.61). The integral (5.16) is written, in the t-u-v coordinate system of Fig. 2.6, as

$$I_2 = \int_{t_b}^{t_a} \int_0^{f_c(t)} \frac{(\beta t + \gamma u)^2}{(\sqrt{t^2+u^2})^3}\, dudt + \int_{t_a}^{t_c} \int_0^{f_b(t)} \frac{(\beta t + \gamma u)^2}{(\sqrt{t^2+u^2})^3}\, dudt \tag{5.17}$$

where β and γ are the components of the vector $(x-x_p)$ in the t and u directions, respectively. Let $f(t) = mt + n$. The integrals (5.17) are of the form

$$I = \int_0^T \int_0^{mt+n} \frac{(\beta t + \gamma u)^2}{(\sqrt{t^2+u^2})^3}\, dudt \tag{5.18}$$

which has the closed-form expression given by

$$I = (\sqrt{(m^2+1)T^2+2mnT+n^2} - |n|)\ [\frac{m\beta^2-2\beta\gamma-m\gamma^2}{m^2+1}] + [\frac{\beta^2-n\gamma^2}{\sqrt{m^2+1}}$$

$$- \frac{mn}{\sqrt{m^2+1}}(m\beta^2-2\beta\gamma-m\gamma^2)]\ [\sinh^{-1}\frac{(m^2+1)T+mn}{|n|} - \sinh^{-1}\frac{mn}{|n|}$$

$$+ T\sinh^{-1}(\frac{n}{T}+m) + \frac{n}{\sqrt{m^2+1}}\{\ell n|\sqrt{m^2+1}\ [(m^2+1)T^2+2mnT+n^2]^{\frac{1}{2}}$$

$$+ (m^2+1)T+mn| - \ell n|\sqrt{m^2+1}\ |n| + mn|\} \qquad (5.19)$$

Equation (5.19) is the basic expression used to compute the integral (5.17).

5.4 AN EXAMPLE — A SPHERICAL CAVITY

Consider the problem of finding the displacement field for a spherical cavity centred at the origin with prescribed displacements u_1, u_2 and u_3 at the surface r = 1 given by [45]

$$u_\alpha = C\, x_\alpha x_3 \qquad \alpha = 1,2$$

$$u_3 = C(\frac{\lambda+3}{\lambda+\mu} + x_3^2) \qquad (5.20)$$

where, for copper (which is the case considered here), $\lambda = 11.82 \times 10^6$ psi and $\mu = 5.6 \times 10^6$ psi are the Lamé constants and

$$C = \frac{\lambda+\mu}{8\pi\mu(\lambda+2\mu)}$$

From (5.8), the equation to be solved is

$$\int_R \bar{\bar{G}}(s|s')\cdot\bar{f}(s')\,ds' = \bar{u}(s) \qquad (5.21)$$

From symmetry, the problem is solved over one-eighth of the spherical surface. Fig. 5.1 shows the finite-element model used. With N = 1, there are seven nodes each having three components of $\bar{f}$ as the unknown variables. This results in a total number of 21 unknowns which is three times that of an analogous scalar problem. For quadratic approximation,

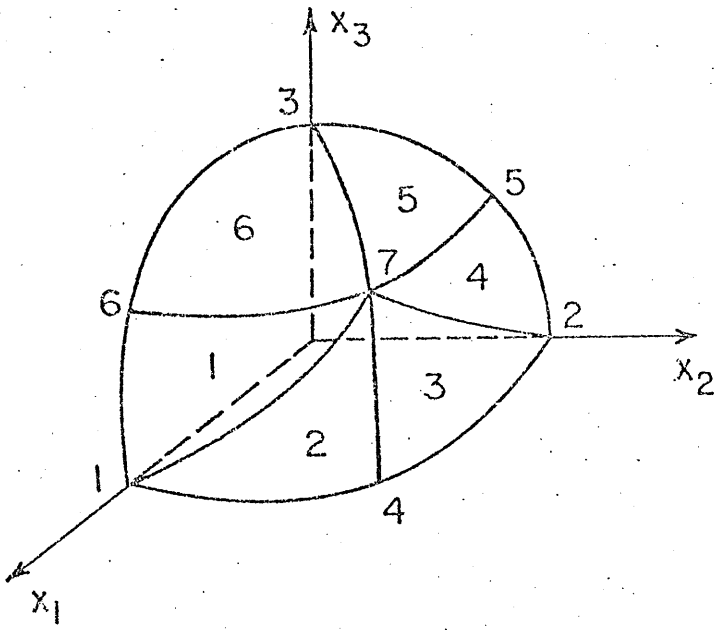

Fig. 5.1 The finite-element model of the spherical cavity

TABLE 5.1

The sphere - displacement at x=z=0, y=2
in units of 10^{-8} inches

Order of approximation	No. of variables	Integral equation solution		Exact solution
		Planar elements	Isoparametric	
1	21	$\begin{bmatrix} 0. \\ 10^{-19} \\ 0.39615 \end{bmatrix}$	$\begin{bmatrix} 0. \\ 10^{-19} \\ 0.39615 \end{bmatrix}$	$\begin{bmatrix} 0. \\ 0. \\ 0.44168 \end{bmatrix}$
2	57	$\begin{bmatrix} 0. \\ 10^{-19} \\ 0.39872 \end{bmatrix}$	$\begin{bmatrix} 0. \\ 10^{-19} \\ 0.43847 \end{bmatrix}$	

six nodes are associated with each element. This results in a total number of 19 nodes or 57 variables for the model used.

The exact solution of the displacements is given by [45]

$$u_\alpha = C \frac{x_\alpha x_3}{r} \qquad \alpha = 1,2$$

$$u_3 = C\left(\frac{\lambda+3}{\lambda+\mu} \frac{1}{r} + \frac{x_3^2}{r^3}\right) \tag{5.22}$$

where $r = [(x_1-x_1')^2 + (x_2-x_2')^2 + (x_3-x_3')^2]^{\frac{1}{2}}$ with $x_1'=x_2'=x_3'=0$. The displacements at an arbitrary point $x_1=x_3=0$ and $x_2=2$ are calculated and given in Table 5.1. Considerable improvement in accuracy is observed by using the second order elements as compared to the first order approximation.

CHAPTER VI

CONCLUSION

A new numerical method — a generalization of the isoparametric finite-element method — has been presented for the solution of boundary integral equation formulation of three-dimensional fields. The formulation of boundary-value problems in terms of integral equations defined on boundary surfaces effectively reduces the dimension of the problem by one. Thus, in solving a three-dimensional problem, the numerical discretization is to be performed only on the bounding surface which is essentially a two-dimensional region. The results obtained for a number of illustrative examples in various fields justify the technique. Its applicability is demonstrated to both the scalar and vector fields formulated in terms of Fredholm integral equations of the first and the second kinds.

The finite-element method is flexible and convenient. Boundary surfaces may be taken as a single element or may conveniently be divided into elements of arbitrary sizes. One is thus able to concentrate on regions of particular interest. The two-parameter, nonplanar element provides a high-order modelling of curved surfaces with a consequent reduction in the significant but often neglected geometrical modelling error. These curved elements generated from the isoparametric mapping reduce the number of elements required for a given degree of approximation.

This means smaller matrix size as compared to current methods which involve planar rectangular subareas and which reduce the geometrical modelling error by increasing the number of subareas. Moreover, the use of the isoparametric mapping allows all numerical integrations over three-dimensional surface elements to be performed over a simple two-dimensional simplex and facilitates the development of a fully automated general algorithm. A computer program, coded in FORTRAN, has been developed. The entire procedure is of general purpose in nature. Problems with arbitrary configurations can be handled with ease.

The polynomial approximation over each finite element has been shown, using the electrostatic T-plate example, to produce an accuracy which would be produced by a constant-pulse point-matching solution using twice as many variables. Furthermore, results indicate that, using identical polynomial trial functions, the variational approach requires a smaller system of linear equations than would the point-matching method for the same accuracy. It has also been shown that, analogous to the self-adjoint operator case, for nonself-adjoint operators, the system of equations derived from the Rayleigh-Ritz procedure is identical to those that would be obtained by the Galerkin method. The elements developed ensure continuity of the function between elements. If continuities of derivatives are required, elements such as the Hermitian element (e.g. [49]) may be constructed.

The matrix system resulting from the discretization of the integral equation is dense. This is unfavourable as compared to the sparse system of the partial differential equation approach. Depending on the individual situations considered, approximations such as neglecting

the contribution of distant elements may be made to yield a simplified system. Since the size of the problems considered is relatively small, a direct method of solution by Gaussian triangularization was used to solve the linear equations. Depending on the order of magnitudes of the matrix entries and the size of the system, preconditionings of the matrix system such as normalizing and scaling, may be needed to avoid a faulty termination of the equation-solving process. For large systems, the dense matrix equations may be handled by, for example, a banded matrix iterative solution method [37] which decomposes a matrix S into the sum of three components as

$$S = L + B + U$$

where B is a banded matrix and U and L are the lower and upper triangular matrices, respectively. The matrix equation

$$S\underline{x} = \underline{b}$$

can then be written as

$$B\underline{x}_{i+1} = \underline{b} - (L+U)\underline{x}_i$$

Thus a banded system is solved at each iterative stage. The method has been reported to be more efficient than the Gaussian elimination method. To accomodate situations where the core-memory requirement exceeds the available capacity, an iterative procedure which solves iteratively one subregion at a time of the entire structure is described in Chapter II. For each subregion under consideration, the unknowns

associated with the remaining subregions are assumed to be known. In this case, one is solving, in terms of core-memory requirement, a problem of size corresponding to that of a single subregion (which may consist of one or more elements).

The generation of the matrix entries involves the evaluation of double surface integrals which is an expensive operation. To economize computation, for distant elements, a quadrature formula of lower order may be used. Alternatively, instead of performing integrations numerically, Csendes [46] derived an approximate closed-form expression for the functional corresponding to the integral constraint on the boundary of a two-dimensional exterior region satisfying Laplace's equation. As a result, the required integration is replaced by the evaluation of a few logarithms and a few simple matrix operations. The saving in computation is significant.

Analogous to the isoparametric integral finite elements, two types of volume elements, the cube and the prism, were described for computing the free-space magnetic field due to current sources. All integrations were done in local coordinates. The algorithm is thus applicable to conductors of any configurations and is of use whenever analytical integrations are not possible. Gaussian quadrature of order 11 is observed adequate in all computation. For points distant from the coil, lower-order quadrature formulas can be used. It has been brought to the author's attention recently that an algorithm described in [48] for computing the demagnetization tensor, using a semi-closed form expression, is applicable and would probably be more efficient than performing all integrations numerically.

The coupling of partial differential equations and integral equations is an effective formulation for problems involving open regions with local inhomogeneities. Reference [7] reported an approach where the constraint equations resulting from a point-matching discretization of an integral equation is coupled to the variational discretized system of the partial differential equation. It is pointed out in [10] that the mutual constraint of the partial differential and the integral formulations both in a variational form is felt likely to produce better results. In view of the finite-element integral approach developed, partial differential equation and integral equation formulations may be constrained in a variational fashion and solution with high accuracy is expected. This bears further investigation.

For nonlinear problems, one may obtain a solution through an iterative procedure based on the algorithm developed in this work. The effect of saturation may be included as a source field and the volume integration scheme of Section 4.3 is applicable directly. The approach therefore does not involve discretization over a volumetric region and the essential property of boundary integral formulations is preserved.

The single-field formulation of Chapter IV, in which the interface constraint equations and the governing integral equation derived from the Green's theorem are combined to yield a single equation in the magnetic scalar potential ϕ, results in a smaller system and is a preferable formulation if only the field in the interior region is of interest. It is concluded that whenever exterior fields are to be found, a two-field

formulation in which both the potential and its normal derivatives are interpolated independently must be used. Alternatively, a boundary formulation in vector potential may, perhaps, also prove promising. This needs further investigation.

The object of this thesis has been to achieve a generalization of the finite-element concept to include its application to the solution of integral equations. In view of this work, the term "finite elements", which has been generally understood to mean the application of that technique to the solution of partial differential equations exclusively, is to be understood in a more general context. It covers the application of the technique to both partial differential and integral equations.

REFERENCES

[1] O.D. Kellogg, Foundations of Potential Theory, New York: Ungar, 1929.

[2] M.A. Jaswon, "Integral equation methods in potential theory I", Proc. Roy. Soc. Lond. A275, pp. 23-32, 1963.

[3] G.T. Symm, "Integral equation methods in potential theory II", Proc. Roy. Soc. Lond. A275, pp. 33-46, 1963.

[4] I. Stakgold, Boundary Value Problems of Mathematical Physics, vol. II, New York: MacMillan, 1968.

[5] I.A. Cermak and P. Silvester, "Solution of 2-dimensional field problems by boundary relaxation", Proc. IEEE, vol. 115, pp. 1341-1348, 1968.

[6] F. Sandy and J. Sage, "Use of finite difference approximations to partial differential equations for problems having boundaries at infinity", IEEE Trans. Microwave Theory Tech., vol. MTT-19, pp. 484-485, May 1971.

[7] B.H. McDonald and A. Wexler, "Finite-element solution of unbounded field problems", IEEE Trans. Microwave Theory Tech., vol. MTT-20, pp. 841-847, Dec. 1972.

[8] C.G. Williams and G.K. Cambrell, "Efficient numerical solution of unbounded field problems", Electron. Lett., vol. 8, pp. 247-248, 1972.

[9] P. Silvester and M.S. Hsieh, "Finite-element solution of 2-dimensional exterior field problems", Proc. IEEE, vol. 118, pp. 1743-1747, Dec. 1971.

[10] B.H. McDonald and A. Wexler, "Mutually constrained partial differential and integral equation field formulations" in Finite Elements in Electrical and Magnetic Field Problems, M.V.K. Chari and P. Silvester (eds.), New York: Wiley, 1977.

[11] O.C. Zienkiewicz and Y.K. Cheung, "Finite-elements in the solution of field problems", The Engineer, pp. 507-510, Sept. 1965.

[12] O.C. Zienkiewicz, The Finite Element Method in Engineering Science, London: McGraw-Hill, 1971.

[13] S.G. Mikhlin, Variational Methods in Mathematical Physics, New York: MacMillan, 1964.

[14] R.F. Harrington, Field Computation by Moment Methods, New York: MacMillan, 1968.

[15] F.J. Rizzo, "An integral equation approach to boundary value problems of classical elastostatics", Q. Appl. Math., vol. 25, no. 1, pp. 83-95, 1967.

[16] T.A. Cruse, "Numerical solutions in three-dimensional elastostatics", Int. J. Solids Structures, vol. 5, pp. 1259-1274, 1969.

[17] T.A. Cruse, "Application of the boundary-integral equation method to three-dimensional stress analysis", Computer & Structures, vol. 3, pp. 509-527, 1973.

[18] L.G. Copley, "Integral equation method for radiation from vibrating bodies", J. Acoust. Soc. Am., vol. 41, no. 4, pp. 807-816, 1967.

[19] H.A. Schenck, "Improved integral formulation for acoustic radiation problems", J. Acoust. Soc. Am., vol. 44, no. 1, pp. 41-58, 1968.

[20] S.C. Wu and Y.L. Chow, "An application of the moment method to waveguide scattering problems", IEEE Trans. Microwave Theory Tech., vol. MTT-20, no. 11, pp. 744-749, Nov. 1972.

[21] A.J. Poggio and E.K. Miller, "Integral equation solutions of three-dimensional scattering problems", in Computer Techniques for Electromagnetics, R. Mittra (ed.), New York: Pergamon Press, 1973.

[22] J.H. Richmond, "TE-wave scattering by a dielectric cylinder of arbitrary cross-section shape", IEEE Trans. Antennas Propagation, vol. AP-14, no. 4, pp. 460-464, July 1966.

[23] T.A. Cruse, "An improved boundary-integral equation method for three-dimensional elastic stress analysis", Computers & Struct., vol. 4, pp. 741-754, 1974.

[24] P. Silvester and M.S. Hsieh, "Projective solution of integral equations arising in electric and magnetic field problems", Int. J. Comput. Phys., vol. 8, pp. 78-82, 1971.

[25] B.H. McDonald, M. Friedman and A. Wexler, "Variational solution of integral equations", IEEE Trans. Microwave Theory Tech., vol. MTT-22, pp. 237-248, March 1974.

[26] G. Jeng and A. Wexler, "Self-adjoint variational formulation of integral equations for scalar field problems", to be published in IEEE Trans. Microwave Theory Tech..

[27] J.C. Lachat and J.O. Watson, "Effective numerical treatment of boundary integral equations: a formulation for three-dimensional elastostatics", Int. J. for Numerical Methods in Engineering, vol. 10, no. 5, pp. 991-1005, 1976.

[28] G. Jeng and A. Wexler, "Finite-element solution of boundary integral equations", in Proceeding of the International Symposium on Large Engineering Systems, August 9 to 12, 1976, A. Wexler(ed.), Pergamon Press, New York, N.Y., pp. 112-121, 1977.

[29] G. Jeng and A. Wexler, "Isoparametric, finite-element, variational solution of integral equations for three-dimensional fields", Int. J. for Numerical Methods in Engineering, vol. 11, 1977.

[30] J.R. Westlake, A Handbook of Numerical Matrix Inversion and Solution of Linear Equations, New York: Wiley, 1968.

[31] A. Wexler, "Computation of electromagnetic fields" (Invited paper), IEEE Trans. Microwave Theory Tech., vol. MTT-17, pp. 416-439, Aug. 1969.

[32] L.V. Kantovich and V.I. Krylov, Approximate Methods of Higher Analysis, New York: Interscience Publishers Inc., 1964.

[33] A.H. Stroud and D. Secrest, Gaussian Quadrature Formulas, Prentice-Hall Inc., Englewood Cliffs, N.J., 1966.

[34] A. Shoamanesh and L. Shafai, "An approximate method for investigation of large circular loop arrays", in Proceedings of the International Syposium on Large Engineering Systems, August 9 to 12, 1976, A. Wexler (ed.), Pergamon Press, New York, N.Y., pp. 129-138, 1977.

[35] G.E. Forsythe and C.B. Moler, Computer Solution of Linear Algebraic Systems, Englewood Cliffs, N.J.: Prentice-Hall, 1967.

[36] A. Sankar and T.C. Tong, "Current computation on complex structures by finite-element method", Electronics Letter, vol. 11, no. 20, pp. 481-482, 1975.

[37] T.R. Ferguson, T.H. Lehman and R.J. Balestri, "Efficient solution of large moment problems: Theory and small problem results", IEEE Trans. Antennas Propagation, vol. AP-24, no. 2, pp. 230-235, March 1976.

[38] A.N. Tikhonov and A.A. Samarskii, Equations of Mathematical Physics, New York: MacMillan, 1963.

[39] J.A. Stratton, Electromagnetic Theory, New York: McGraw-Hill, 1941.

[40] J. Van Bladel, Electromagnetic Fields, New York: McGraw-Hill, 1964.

[41] C.W. Trowbridge, "Application of integral equation methods for the numerical solution of magnetostatic and eddy current problems", in Finite Elements in Electrical and Magnetic Field Problems, M.V.K. Chari and P. Silvester (eds.), New York: Wiley, 1977.

[42] R.H. Gallagher, Finite-Element Analysis Fundamentals, Englewood Cliffs, N.J.: Prentice-Hall Inc., 1975.

[43] G. Strang and G. Fix, An Analysis of the Finite Element Method, Englewood Cliffs, N.J.: Prentice-Hall Inc., 1973.

[44] A.E.H. Love, A Treatise on the Mathematical Theory of Elasticity, New York: Dover, 1944.

[45] I.S. Sokolnikoff, Mathematical Theory of Elasticity, New York: McGraw-Hill, 1956.

[46] Z.J. Csendes, "A note on the finite-element solution of exterior-field problems", IEEE Trans. on Microwave Theory and Techniques, vol. MTT-24, no. 7, pp. 468-473, July 1976.

[47] A. Wexler, "Perspectives on the solution of simultaneous equations", in Finite Elements in Electrical and Magnetic Field Problems, M.V.K. Chari and P. Silvester (eds.), New York: Wiley, 1977.

[48] C.J. Hegedus, G. Kadar and E. Della Torre, "Demagnetization tensors for cylindrical bodies", Internal Reports in Simultion, Optimization and Control, McMaster University, No. SOC-141, December 1976.

[49] M.T. Van Genuchten and G.F. Pinder, "Simulation of two-dimensional contaminant transport with isoparametric Hermitian finite-elements", Water Resources Research, vol. 13, no. 2, pp. 451-458, April 1977.